Human Molecular Genetics, 2017, Vol. 26, No. 6 1115–1132

doi: 10.1093/hmg/ddx021
Advance Access Publication Date: 19 January 2017
Original Article

ORIGINAL ARTICLE

A novel humanized mouse model of Huntington disease for preclinical development of therapeutics targeting mutant huntingtin alleles

Amber L. Southwell[1], Niels H. Skotte[1,2], Erika B. Villanueva[1], Michael E. Østergaard[3], Xiaofeng Gu[4], Holly B. Kordasiewicz[3], Chris Kay[1], Daphne Cheung[1], Yuanyun Xie[1], Sabine Waltl[1], Louisa Dal Cengio[1], Hailey Findlay-Black[1], Crystal N. Doty[1], Eugenia Petoukhov[1], Diepiriye Iworima[1], Ramy Slama[1], Jolene Ooi[5], Mahmoud A. Pouladi[5,6], X. William Yang[4], Eric E. Swayze[3], Punit P. Seth[3] and Michael R. Hayden[1,*]

[1]Centre for Molecular Medicine and Therapeutics, Child and Family Research Institute, University of British Columbia, Vancouver, BC, Canada, [2]Novo Nordisk Foundation Center for Protein Research, Faculty of Health and Medical Sciences, University of Copenhagen, Copenhagen, Denmark, [3]IONIS Pharmaceuticals, Carlsbad, CA, USA, [4]Center for Neurobehavioral Genetics, Semel Institute for Neuroscience and Human Behavior; Department of Psychiatry and Biobehavioral Sciences, University of California, Los Angeles, CA, USA, [5]Translational Laboratory in Genetic Medicine, Agency for Science, Technology and Research and the Department of Medicine, National University of Singapore, Singapore 138648 and [6]Department of Medicine, Yong Loo Lin School of Medicine, National University of Singapore, Singapore 117597

*To whom correspondence should be addressed at: Centre for Molecular Medicine and Therapeutics, Child and Family Research Institute, University of British Columbia, 950 W 28th Avenue, Vancouver, BC v5z 4h4, Canada. Tel: +1 6048753535; Fax: +1 6048753819; Email: mrh@cmmt.ubc.ca

Abstract

Huntington disease (HD) is a neurodegenerative disease caused by a mutation in the huntingtin (*HTT*) gene. HTT is a large protein, interacts with many partners and is involved in many cellular pathways, which are perturbed in HD. Therapies targeting HTT directly are likely to provide the most global benefit. Thus there is a need for preclinical models of HD recapitulating human *HTT* genetics. We previously generated a humanized mouse model of HD, Hu97/18, by intercrossing BACHD and YAC18 mice with knockout of the endogenous mouse HD homolog (*Hdh*). Hu97/18 mice recapitulate the genetics of HD, having two full-length, genomic human *HTT* transgenes heterozygous for the HD mutation and polymorphisms associated with HD in populations of Caucasian descent. We have now generated a companion model, Hu128/21, by intercrossing YAC128 and BAC21 mice on the *Hdh*−/− background. Hu128/21 mice have two full-length, genomic human HTT transgenes heterozygous for the HD mutation and polymorphisms associated with HD in populations of East Asian descent and in a minority of patients from other ethnic groups. Hu128/21 mice display a wide variety of HD-like phenotypes that are similar to YAC128 mice. Additionally, both transgenes in Hu128/21 mice match the human HTT exon 1 reference sequence. Conversely,

Received: October 20, 2016. **Revised:** December 23, 2016. **Accepted:** January 10, 2017

the BACHD transgene carries a floxed, synthetic exon 1 sequence. Hu128/21 mice will be useful for investigations of human HTT that cannot be addressed in Hu97/18 mice, for developing therapies targeted to exon 1, and for preclinical screening of personalized HTT lowering therapies in HD patients of East Asian descent.

Introduction

Huntington disease (HD) is an autosomal dominant neurodegenerative disease caused by the pathogenic expansion of a polyglutamine (PolyQ) encoding CAG tract in exon 1 of the huntingtin (*HTT*) gene to greater than 35 repeats (1). The *HTT* gene is pleiotropic likely because the HTT protein has many interactors and mutant HTT (muHTT) perturbs many cellular pathways resulting in a complex pathogenesis (2,3). The clinical features of HD include psychiatric disturbance, motor and cognitive deficits, weight loss, sleep disturbance and immune hyperactivation (4–6). Moderately effective symptomatic therapies are used in the treatment HD because disease modifying therapies are not available (7). Considering the promiscuous nature of the muHTT protein, therapeutics targeting muHTT directly are likely to provide the most global benefit. A variety of therapeutic strategies targeting muHTT are in development including those targeting the gene, the transcript and the protein. The mouse Huntington disease homolog (*Hdh*) is 86% identical to human HTT at the cDNA level and 91% identical at the protein level (8), suggesting that it may be possible to perform preclinical evaluation of some HTT targeted therapeutics in murine systems. However, some strategies, such as antisense oligonucleotides (ASOs) that recognize intronic polymorphisms (9,10), target regions that are not conserved and require model systems with only human HTT.

There are two HD mouse lines expressing full-length, genomic human HTT; BACHD with 97Q (11) and the YAC series with 18, 46, 72 or 128Q (12,13). We previously intercrossed BACHD and YAC18 mice on the background of *Hdh*−/− to generate a humanized mouse model of HD, Hu97/18 (14). Hu97/18 mice are a unique tool for preclinical studies of human HTT and display a wide range of HD-like behavioral, neuropathological and electrophysiological changes (14,15). Aside from the mutation region, the BACHD and YAC transgenes differ at therapeutically relevant single nucleotide polymorphism (SNP) sites. BACHD mice express human HTT from an A haplogroup *HTT* gene, while the YAC HD mouse lines express human HTT from a C haplogroup *HTT* gene (14). Hu97/18 mice have A haplogroup muHTT from BACHD and C haplogroup wtHTT from YAC18. The A haplogroup is most frequently associated with CAG expansion in populations of Caucasian descent (16,17), and Hu97/18 mice have previously been used for preclinical development of ASOs targeted to A haplogroup polymorphisms for therapeutic allele-specific suppression of muHTT (10,18–20). HTT haplogroup C is most frequently associated with CAG tract expansion in populations of East Asian descent (21), and a humanized mouse line with haplogroup C muHTT (YAC) and haplogroup A wtHTT (BAC) would be useful for developing ASOs targeted to haplogroup C polymorphisms for allele-specific muHTT suppression in HD patients of East Asian descent. In addition, the CAG expansion commonly occurs on the C haplogroup in Black South African HD patients (22), and in a small proportion of European patients that would be untreatable with other priority allele targets tailored to this population (17).

The BACHD and YAC128 mouse models of HD share many characteristics. However, significant phenotypic differences have been reported (23). YAC128 mice display prepulse inhibition deficits, downregulation of HD-associated striatal genes, and robust muHTT inclusions in brain, all of which are consistent with HD and not apparent in BACHD mice (23). As a result, these aspects of HD cannot be investigated in BACHD mice or the derivative Hu97/18 line. Phenotypic differences between BACHD and YAC128 mice may be explained by differences in the respective transgenes. When compared with the BACHD transgene, the YAC128 transgene includes an additional 4 kb upstream and 66.8 kb downstream of the *HTT* gene (23), which may include regulatory regions. Additionally, the BACHD transgene includes a floxed, synthetic exon 1 sequence (11). This provides a powerful research tool, allowing for temporal and tissue-specific inactivation of the transgene by the cre recombinase and subsequent studies on the contribution of select pools of muHTT to the pathogenesis of HD. However, this alteration of the *HTT* gene could also lead to functional differences. Finally, the BACHD CAG repeat region is fully interrupted with CAAs, having only two contiguous CAGs in any location (23). For this reason, therapeutics and reagents targeting the expanded CAG tract cannot be investigated in BACHD mice or the derivative Hu97/18 line. The interrupted CAG tract in the BACHD transgene may also result in loss of or production of non-physiologic repeat-associated-non-ATG (RAN) translation products. RAN proteins are toxic and thought to contribute to the pathogenesis of HD (24), so their loss could diminish or abolish certain HD-like changes. The YAC128 repeat region is less interrupted, containing only nine CAA repeats and 116 CAG repeats. Moreover, there is a contiguous stretch of 80 CAGs from repeat 29 to repeat 109 (23), suggesting that YAC128 mice, or derivative humanized lines, could be used for studies requiring expanded CAG or RAN translation.

To provide a humanized HD mouse model for studies of HTT exon 1, HTT with contiguous expanded CAG, or mu*HTT* on haplogroup C, we first required a mouse line with wt*HTT* on haplogroup A. We generated a BAC21 transgenic mouse line expressing full-length, genomic A haplogroup human wt*HTT* with no synthetic alterations to the gene sequence. BAC21 mice were then intercrossed to YAC128 mice on the *Hdh*−/− background to generate a new humanized HD mouse line, Hu128/21. We have characterized Hu128/21 mice for HD-like behavioral, neuropathological, biochemical and striatal gene expression changes. Additionally, in a proof of concept study, we have used Hu128/21 mice to screen ASOs targeted to HTT haplogroup C polymorphisms for allele-specific suppression of muHTT.

Results

Hu128/21 mice can be used to evaluate therapeutics targeted to human HTT exon 1

Direct sequencing of exon 1 of the BACHD transgene revealed that it differs from the human HTT reference sequence at 31 positions outside of the CAG repeat region (Supplementary Material, Fig. S1). Each of these changes is silent at the amino acid level and 26 of 31 changes are G/C to A/T substitutions, which would reduce GC content of the synthetic, floxed exon 1 sequence. Although this does not affect protein targeted

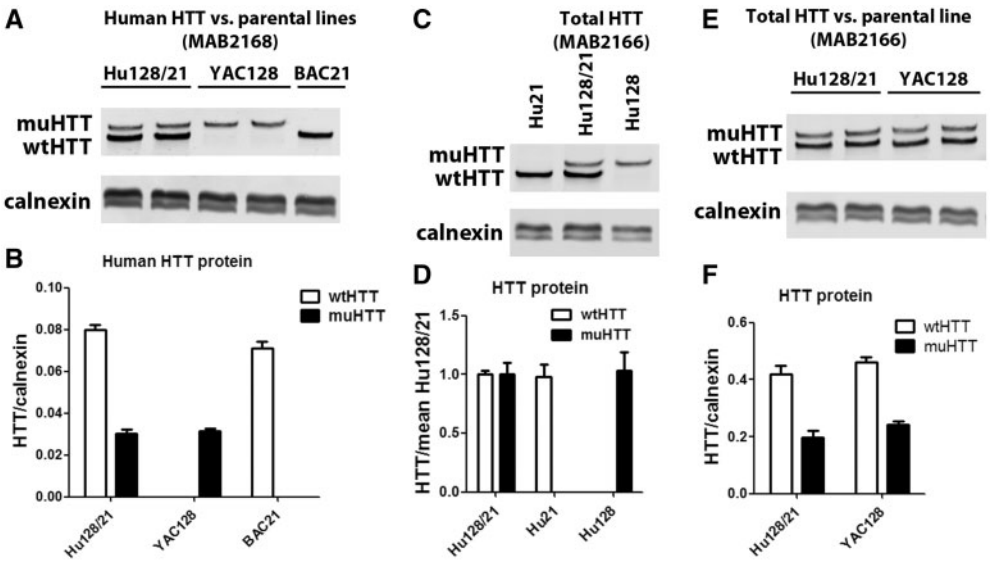

Figure 1. Cortical HTT protein levels in Hu128/21 mice. Total protein was isolated from cortices of 4-month-old animals and assessed for HTT levels by allelic separation immunoblotting. **(A, B)** Human HTT in Hu128/21 brain was compared with the founder lines, YAC128 and BAC21 demonstrating no changes in transgenic protein after humanization. **(C, D)** Total HTT levels were compared in Hu128/21, Hu21 and Hu128 mice demonstrating no change in HTT levels after interbreeding. **(E, F)** Total HTT levels in Hu128/21 were compared with YAC128 mice demonstrating that the ratio of wt and muHTT in these two lines is similar. (A, C, E) Representative immunoblots. (B, D, F) Quantitation from an number of four animals per genotype.

therapeutics, reagents targeted to exon 1 DNA or transcripts, such as HTT miRNAs (25) will likely not recognize BACHD exon 1. As a result, our previously generated humanized HD mouse line, Hu97/18, which carries muHTT from the BACHD transgene, cannot be used to evaluate therapeutics targeted to human HTT exon 1. Conversely, the BAC21 transgene is a perfect match to the human HTT exon 1 reference sequence (Supplementary Material, Fig. S1), meaning that Hu128/21 mice can be used for preclinical studies of reagents targeting human HTT exon 1.

HTT levels in Hu128/21 mice are similar to those in YAC128 mice

Cortical HTT protein was assessed in 4-month-old animals by allelic separation immunoblotting. Comparison of human HTT levels in Hu128/21 and parental lines YAC128 and BAC21 demonstrate that human muHTT levels are similar in Hu128/21 and YAC128 brain and that human wtHTT levels are similar in Hu128/21 and BAC21 brain (Fig. 1A and B). This indicates no change in transgene levels by humanization. Comparison of total cortical HTT protein in Hu21, and Hu128 humanized founder lines vs. Hu128/21 mice revealed that intercrossing did not result in changes in transgenic HTT level (Fig. 1C and D). Comparison of total cortical HTT levels in Hu128/21 and YAC128 mice demonstrates that wt and muHTT levels are similar in these lines (Fig. 1E and F). When compared with the parental BACHD line, Hu97/18 mice have reduced BACHD-derived muHTT and a concomitant delay in onset or reduction in severity of some HD-like phenotypes (14). Although the mechanism of this downregulation remains unknown, similar brain muHTT levels between Hu128/21 mice and the parental YAC128 line suggests that it is not the result of humanization. Additionally, because phenotypic severity of HD mouse lines is tightly linked to muHTT levels (26), these results indicate that HD-like phenotypes in Hu128/21 mice will likely be similar to those observed in YAC128 mice.

Hu128/21 mice display weight gain and testicular atrophy

Weight loss is a feature of HD (5). However, YAC128 and BACHD mice display weight gain (11,27). To evaluate body weight in the Hu128/21 line, Hu128/21 and Hu21 littermate controls were weighed at 2-month intervals from 2 to 12 months of age. Comparison to historical age matched FVB/N body weight data demonstrates that Hu128/21 males are significantly overweight (genotype effect $P < 0.0001$) with *post hoc* differences observed at 6 and 12 months of age (Fig. 2A). Weight gain was more pronounced in female mice with both Hu21 and Hu128/21 mice showing significant weight gain from 4 months of age (Fig. 2B). These results are consistent with Hu97/18 mice, which display weight gain in both HD and control lines and greater magnitude weight gain in females (14) and with YAC128 mice, which display weight gain that is greater in females (28).

Testicular degeneration is a feature of HD that is recapitulated in YAC128 mice (29). To evaluate this measure in Hu128/21 mice, weight of post-perfusion testes were scored at 3, 6, 9 or 12 months of age. Although testis weight was found to decline with age in both Hu128/21 and Hu21 mice (age effect $P < 0.0001$), this decline was exacerbated in Hu128/21 mice (genotype effect $P < 0.0001$). When compared with Hu21 littermate controls Hu128/21 mice displayed smaller testis by *post hoc* analysis from 9 months of age (Fig. 2C). YAC128 mice do not display smaller testis than WT littermates until 12 months of age (29). This analysis was also performed in Hu97/18 and Hu18/18 mice to allow comparison. Although testis weight was found to decline with age in both genotypes (age effect $P = 0.01$), no effect of genotype was observed (genotype effect $P = 0.6354$) (Fig. 2D).

Hu128/21 mice display progressive motor deficits

Motor deficits are a cardinal feature of HD that define clinical onset (30), and YAC128 mice display progressive motor deficits (12). Hu128/21 mice were evaluated for motor learning during

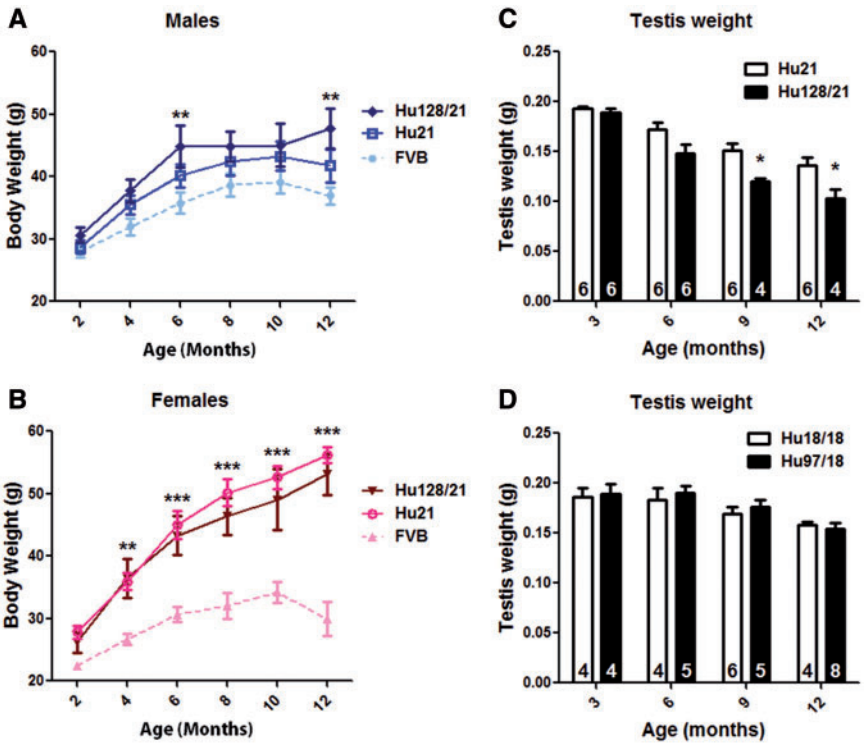

Figure 2. Hu128/21 mice display weight gain and testicular degeneration. Mice were weighed at 2-month intervals from 2 to 12 months of age. **(A)** Male Hu128/21 mice were significantly heavier than age matched historical FVB mice (14) at 6 and 12 months of age. **(B)** Female Hu21 and Hu128/21 mice displayed greater magnitude weight gain than males and were significantly heavier than age matched FVB mice from 4 months of age. Post-perfusion testis was weighed at the indicated ages. **(C)** Testis weight declines with age in both Hu21 and Hu128/21 mice, but decline is greater in Hu128/21 mice leading to significantly smaller testis from 9 months of age. **(D)** Testis weight declines with age in both Hu18/18 and Hu97/18 mice. No effects of genotype were noted. *Different from Hu21, *$P < 0.05$, **$P < 0.01$, ***$P < 0.001$.

rotarod training at 2 months of age. When compared with Hu21 littermates, Hu128/21 mice fell more frequently with lower latency to the first fall during training (Fig. 2A and B). This may be indicative of a motor learning deficit similar to what has been reported for YAC128 mice (31). However, when considering accelerating rotarod testing only at 2 months of age, Hu128/21 mice had a shorter latency to fall than Hu21 littermates (not significant by Bonferroni *post hoc* analysis of longitudinal data, $P = 0.0320$ by student's *t* test at 2 months of age) (Fig. 3C). This suggests that the poor performance during rotarod training in Hu128/21 mice may be the result of an early onset motor deficit, rather than a deficit in motor learning.

During longitudinal accelerating rotarod testing from 2 to 12 months of age, both Hu21 and Hu128/21 mice displayed progressive decline in motor performance (Fig. 3C). This may be related to the weight gain observed in both genotypes, which would confound motor testing. The performance of Hu128/21 mice was consistently worse than Hu21 littermate controls (genotype effect $P < 0.0001$), though this failed to reach *post hoc* significance at any time point. These results are consistent with the Hu97/18 line for which progressive rotarod deficits have been observed in both HD and control animals, with HD animals demonstrating greater deficit (14).

Mice were evaluated for motor performance during spontaneous climbing at 2 months intervals from 2 to 12 months of age. Climbing performance of both genotypes of mice was found to decline over time with increasing latency to the first climb (Fig. 3D), decreasing number of climbing events (Fig. 3E) and decreasing total time spent climbing (Fig. 3F). No effect of genotype was noted for any of these measures, indicating that this is not an appropriate test for use in this model. Although no genotypic effects were noted in older mice from the Hu97/18 line, at 2 months of age Hu97/18 mice were found to climb significantly less than Hu18/18 littermates (14). Climbing performance also declines with age in YAC128 mice (28). However, because they are compared with WT littermate controls, which perform better in this task than humanized control mice, a substantial genotypic difference is apparent for this measure in the YAC128 line.

Hu128/21 mice display anxiety-like and depressive-like behaviors

Psychiatric disturbance, including anxiety and depression, are features of HD that often precede onset of motor symptoms (32) and are recapitulated in YAC128 (28,33) and other HD model mice (34,35). Mice were evaluated for anxiety during exploration of a brightly lit open field or an elevated plus maze at 3, 6 or 9 months of age. Exploratory activity was found to be normal with no effect of genotype in either paradigm (Fig. 4A and C). Hu128/21 mice were found to display anxiety-like behavior during open field exploration spending significantly less time in the center of the field (genotype effect $P = 0.0008$) with differences reaching *post hoc* significance at 3 and 9 months of age (Fig. 4B). Hu128/21 mice also displayed anxiety-like behavior during elevated plus maze exploration spending significantly less time in the open arms (genotype effect $P = 0.0432$) with differences reaching *post hoc* significance at 9 months of age (Fig. 4D). These results are consistent with YAC128 (28,33) and Hu97/18 (14)

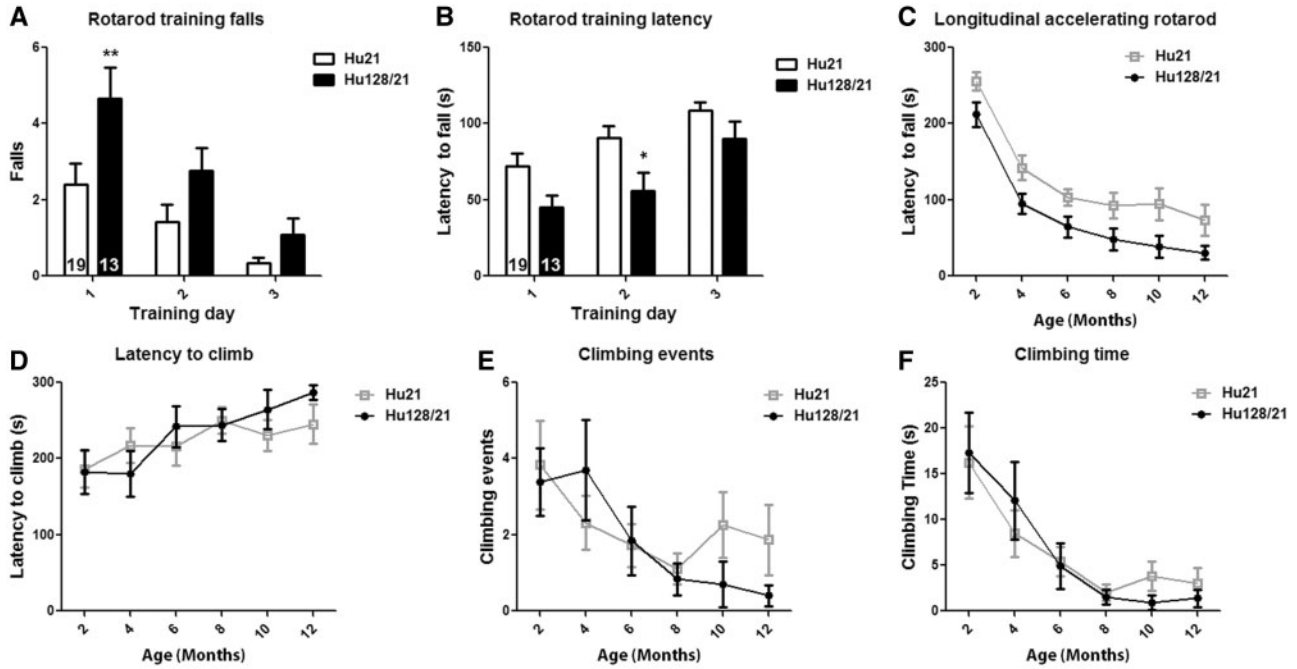

Figure 3. Hu128/21 mice display progressive motor deficits. Motor performance was evaluated longitudinally at 2-month intervals from 2 to 12 months of age using the **(A–C)** accelerating rotarod and **(D–F)** spontaneous climbing tests. (A, B) When compared with Hu21 mice, Hu128/21 (A) fell more frequently and (B) had a reduced latency to the first fall during training on a fixed speed rotarod. (C) Longitudinal rotarod performance of both genotypes progressively declined. Although there was a significant effect of genotype by two-way-ANOVA ($P < 0.0001$), this difference failed to reach significance by *post hoc* analysis at any time point. (D–F) Both genotypes of mice displayed progressive decline in spontaneous climbing during a 5 min exploration of an inverted wire mesh pencil holder as measured by (D) latency to begin climbing, (E) climbing events and (F) total time spent climbing. No effect of genotype was observed for any of these measures. *Different from Hu21, *$P < 0.05$, **$P < 0.01$.

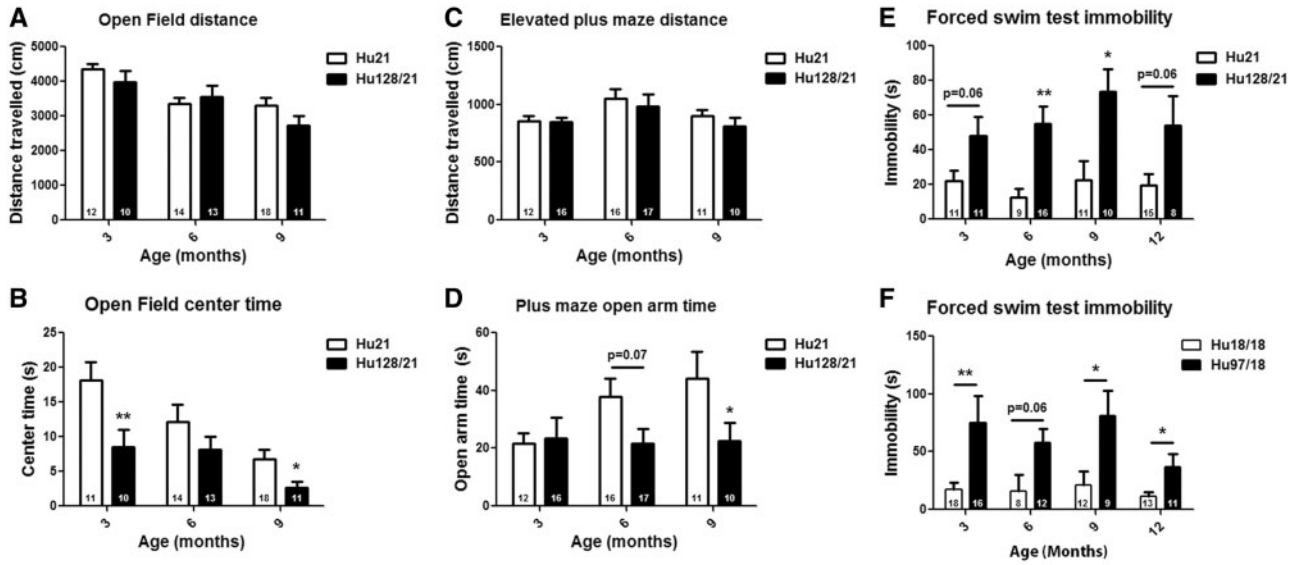

Figure 4. Hu128/21 mice display anxiety- and depressive-like behaviors. **(A, B)** Mice were evaluated during exploration of a brightly lit open field at the indicated ages. (A) Exploratory activity of both genotypes declined with age. However, no genotypic differences were observed. (B) When compared twith Hu21 mice, Hu218/21 mice displayed anxiety-like behavior spending significantly less time in the center of the open field at 3 and 9 months of age with a trend toward reduced center time at 6 months of age. **(C, D)** Mice were evaluated during exploration of an elevated plus maze at the indicated ages. (C) Exploratory activity of both genotypes was similar at all evaluated ages. (D) When compared with Hu21 mice, Hu128/21 mice displayed anxiety-like behavior spending significantly less time in the open arms at 9 months of age with a strong trend toward less open arm time observed at 6 months of age. **(E, F)** Mice were evaluated during forced swimming at the indicated ages. (E) When compared with Hu21 littermates, Hu128/21 mice displayed non-progressive depressive-like behavior, spending significantly more time immobile at 6 and 9 months of age with strong trends toward more time immobile noted at 3 and 12 months of age. (F) When compared with Hu18/18 littermates, Hu97/18 mice displayed non-progressive depressive-like behavior, spending significantly more time immobile at 3, 9 and 12 months of age with strong trends toward more time immobile noted at 6 months of age. Data for Hu97/18 line at 12 months of age were previously reported in (14) and is included here to allow direct comparison. *Different from Hu21 or Hu18/18 same age, *$P < 0.05$, **$P < 0.01$.

mice, which have been previously reported to have normal exploratory activity and increased anxiety-like behaviors during both open field and elevated plus maze exploration.

Depressive-like behavior was evaluated during forced swimming at 3, 6, 9 or 12 months of age. When compared with Hu21 littermate controls, Hu128/21 mice were found to display depressive-like behavior, spending significantly more time immobile (genotype effect $P < 0.0001$), with differences reaching *post hoc* significance at 6 and 9 months of age and strong trends noted at 3 and 12 months of age. No effect of age or interaction of age and genotype was noted (age effect $P = 0.6070$, interaction $P = 0.6750$), indicating that this phenotype is not progressive. This is consistent with what has previously been reported in YAC128 mice (36). This analysis had previously been reported at 12 months of age for Hu97/18 mice demonstrating a depressive-like phenotype (14). To allow comparison, we performed this analysis at 3, 6 or 9 months of age in Hu18/18 and Hu97/18 mice and combined the data with our historical 12-month data. We found that Hu97/18 mice also display non-progressive depressive-like behavior spending significantly more time immobile than Hu18/18 littermates (genotype effect $P < 0.0001$, age effect $P = 0.2803$, interaction $P = 0.6224$) with differences reaching *post hoc* significance at 3, 9 and 12 months of age, and a strong trend observed at 6 months of age (Fig. 4F).

Hu128/21 mice display progressive spatial learning and object recognition deficits

Cognitive deficits often precede motor deficits in HD (37), and this is recapitulated in YAC128 mice (31). Cognition was evaluated in Hu128/21 mice by spontaneous alternation and by object spatial learning and recognition assays. These assays were chosen because they can be performed using only olfactory and tactile clues by physical interaction with objects and the environment and do not rely on sight, which is lost in mice on the FVB/N background strain due to progressive retinal degeneration (38). Spatial learning was assessed at 4 months of age by spontaneous alternation during exploration of a T maze. Although Hu21 mice performed normally, preferentially entering the unexplored arm on the second trial (68% of mice), Hu128/21 mice performed near the level of chance with no preference for the previously unexplored arm (47% of mice) (Fig. 5A left). This is consistent with what has previously been reported for the YAC128 line (39). This test was also performed on Hu97/18 and Hu18/18 littermate controls, and both genotypes demonstrated a preference for the unexplored arm (85% of mice and 71% of mice, respectively) (Fig. 5A right), indicating that at this age and in this paradigm, Hu97/18 mice display intact spatial learning.

Spatial object learning and object recognition were assessed at 3, 6 or 9 months of age by the novel object location and novel object preference assays (Fig. 5B). Hu21 mice displayed intact spatial learning and object recognition at all ages, showing a significant preference for either a known object in a novel location (Fig. 5C, E and G) or for a novel object (Fig. 5D, F and H). Hu128/21 mice displayed a strong trend toward a preference for a known object in a novel location at 3 months of age, but no preference at 6 or 9 months of age (Fig. 5C, E and G), indicating impaired spatial learning. Hu128/21 mice also displayed progressive loss of object recognition, showing a preference for a novel object at 3 months of age, a trend toward a preference at 6 months of age and no preference at 9 months of age (Fig. 5D, F and H). This is similar to what has previously been reported for Hu97/18 mice (14) and YAC128 mice (33).

Hu128/21 mice display progressive forebrain-specific atrophy

Selective forebrain atrophy that is most pronounced in the striatum, but also apparent in the cortex and in white matter (40), is a feature of HD that is recapitulated in YAC128 mice (12,41). Whole brain weight, forebrain weight and cerebellum weight were assessed at 3, 6, 9 or 12 months of age. When compared with Hu21 littermate controls, Hu128/21 mice display reduced whole brain weight at 12 months of age (Fig. 6A) and forebrain weight from 9 months of age (Fig. 6B). There was no effect of genotype on cerebellum weight (Fig. 6C), indicating that atrophy is forebrain-specific, which is consistent with previous reports for 12-months old YAC128 (12) and Hu97/18 mice (14) and with HD, in which the cerebellum is relatively spared (40). When compared with Hu21 littermates, Hu128/21 mice were found to have smaller striata from 3 months of age (genotype effect $P < 0.0001$), the earliest time point evaluated (Fig. 6D). There was no effect of age or interaction of age and genotype in this measure (age effect $P = 0.1064$, interaction $P = 0.7106$), indicating that this phenotype is not progressive, which is contrary to what has previously been reported in YAC128 mice (41) and in HD (42). Cortical volume was significantly lower in Hu128/21 mice than in Hu21 mice (genotype effect $P = 0.0071$). This difference failed to reach *post hoc* significance at any time point evaluated, though a trend toward reduction was observed in Hu128/21 cortices from 3 months of age, the earliest time point evaluated (Fig. 6E). A significant effect of age but no interaction of age and genotype was noted for this measure (age effect $P = 0.0002$, interaction $P = 0.9408$). Corpus callosum volume was significantly reduced in Hu128/21 brain compared with Hu21 brain (genotype effect $P < 0.0001$) reaching *post hoc* significance at 6 and 12 months of age, with trends toward reduction noted at 3 and 9 months of age (Fig. 6F). A significant effect of age but no interaction of age and genotype was noted for this measure (age effect $P = 0.0002$, interaction $P = 0.7176$).

In order to compare the natural history of forebrain atrophy in humanized lines, we also performed this analysis at 3, 6 or 9 months of age in Hu97/18 and Hu18/18 littermate controls and combined the data with our historical data at 12 months of age. When compared with Hu18/18 littermate controls, Hu97/18 exhibit reduced whole brain (genotype effect $P = 0.0126$) and forebrain weight (genotype effect $P = 0.0007$) reaching *post hoc* significance at 12 months of age (Fig. 6G and H). There was no effect of genotype on cerebellum weight (Fig. 6I), indicating that, similar to Hu128/21 mice, atrophy is forebrain-specific. When compared with Hu18/18 littermates, Hu97/18 display progressive striatal (genotype effect $P < 0.0001$, age effect $P = 0.0021$, interaction $P = 0.0021$) and cortical (genotype effect $P < 0.0001$, age effect $P = 0.0043$, interaction $P = 0.0043$) volume loss reaching *post hoc* significance at 9 and 12 months of age (Fig. 6J and K). Corpus callosum volume was significantly less in Hu97/18 brain than in Hu18/18 brain (genotype effect $P = 0.0093$) reaching *post hoc* significance at 9 months of age, with a trend toward reduction noted at 12 months of age (Fig. 6L). No effect of age or interaction of age and genotype was noted for this measure (age effect $P = 0.6556$, interaction $P = 0.6556$).

Hu128/21 mice display HD-like histological changes in the brain

Loss of striatal dopamine- and cAMP-regulated neuronal phosphoprotein (DARPP-32) immunoreactivity, which is a marker of healthy striatal medium spiny neurons, and deposition of muHTT containing inclusions in the brain are features of HD (43,44) that are recapitulated in YAC128 mice (12,45). Striatal DARPP-32 immunoreactivity

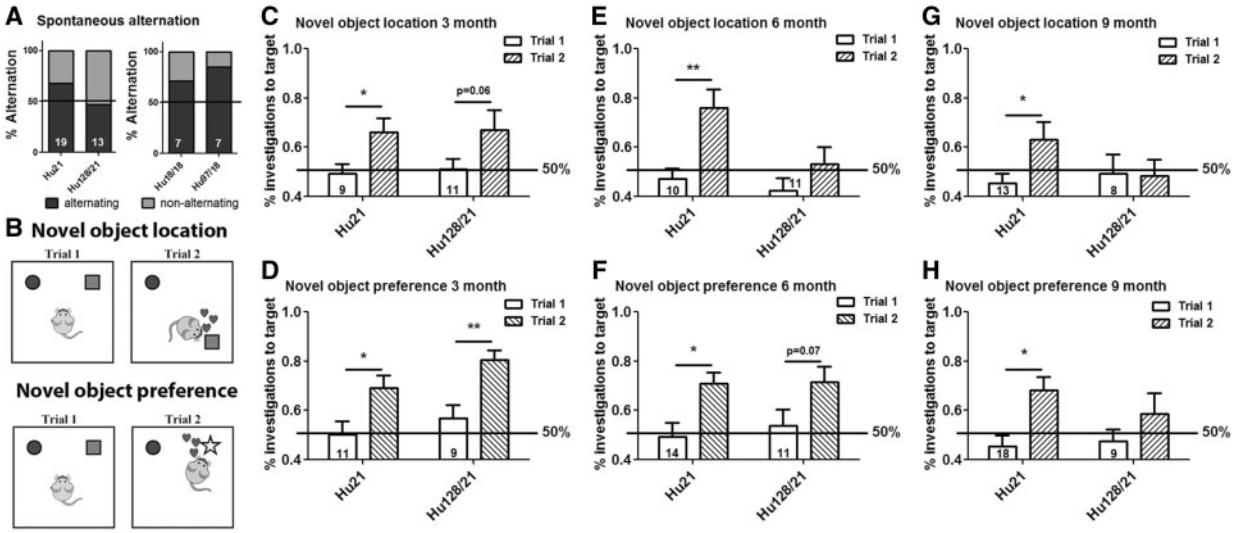

Figure 5. Hu128/21 mice display progressive spatial and object recognition learning deficits. **(A)** Four-month-old mice were evaluated in the spontaneous alternation test of spatial learning. Hu21 mice showed a preference for entering the previously unexplored arm, while Hu128/21 mice showed no arm preference, indicating impaired spatial learning. Hu18/18 and Hu97/18 mice both preferentially entered the unexplored arm, indicating no deficit in this paradigm. Mice were tested at the indicated ages in the **(B)** novel object location test of spatial learning and the novel object preference test of object recognition. **(C, D)** At 3 months of age both genotypes of mice show a preference for the target object, (C) the one in the new location or (D) the novel object, indicating intact spatial learning and object recognition at this age. **(E, F)** At 6 months of age Hu21 mice perform both tasks well, while Hu128/21 mice display (E) disrupted spatial learning but (F) intact object recognition. **(G, H)** At 9 months of age Hu21 mice perform both tasks, indicating intact learning, which Hu128/21 display deficits in both tasks, indicating impaired spatial learning and object recognition. *Difference between indicated columns, *$P < 0.05$, **$P < 0.01$.

was quantified by integrated optical density at 3, 6, 9 or 12 months of age. When compared with Hu21 littermate controls, Hu128/21 mice display reduced striatal DARPP-32 (genotype effect $P = 0.0456$, age effect $P = 0.8763$, interaction $P = 0.8767$). This difference failed to reach *post hoc* significance at any age tested, though a trend toward reduction was noted at 6, 9 and 12 months of age (Fig. 7A and B). This is consistent with Hu97/18 mice, in which we previously reported a trend toward reduced striatal DARPP-32 immunoreactivity at 12 months of age (14). To allow comparison of the natural history of DARPP-32 loss in these two lines, we evaluated Hu97/18 and Hu18/18 littermate controls at 3, 6 or 9 months of age and combined the data with our historical data at 12 months of age. Similar to Hu128/21 mice, we observed reduced striatal DARPP-32 immunoreactivity in Hu97/18 mice (genotype effect $P = 0.0135$, age effect $P = 0.5247$, interaction $P = 0.4965$) that did not reach *post hoc* significance at any age, but showed trends toward reduction at 6, 9 and 12 months of age (Fig. 7C).

muHTT inclusions were evaluated at 3, 6, 9 or 12 months of age by EM48 staining, which recognizes aggregated human HTT (46). No staining was observed in Hu21 brain at any age. In Hu128/21 brain diffuse nuclear staining was apparent at 3 months of age. Staining became more intense and condensed with age, resulting in robust striatal and cortical muHTT inclusions at 9 and 12 months of age (Fig. 7D), with regional staining consistent with what has been previously reported for YAC128 mice (12,47). BACHD mice lack robust striatal muHTT inclusions (23), and muHTT in Hu97/18 mice is derived from the BACHD transgene at a lower expression level than the parental line (14). As a result, Hu97/18 mice are not expected to recapitulate this feature of HD.

Hu128/21 mice recapitulate HD-like striatal gene expression changes

Striatal gene expression changes have been extensively characterized in HD (48–52), and YAC128 (52–54) and other HD mice (55–58) recapitulate many of these. Expression of five genes that are downregulated in HD striatum was assessed by RT-qPCR at 3, 6 or 9 months of age (Fig. 8A–E). Glutamate transporter 1 (GLT1) expression was similar in Hu21 and Hu128/21 striata at all ages (genotype effect $P = 0.0686$, age effect $P = 0.0879$) (Fig. 8A). This is consistent with a previous report demonstrating that GLT1 expression is not altered in YAC128 mice (59). When compared with Hu21 littermates, phosphodiesterase 10A (PDE10A) expression was reduced by 7.2% in striata of 9-month-old Hu128/21 mice (genotype effect $P < 0.0001$, age effect $P = 0.0004$, interaction $P = 0.0004$) (Fig. 8B). Dopamine receptor D2 (DRD2) expression was reduced in Hu128/21 striata by 6.9% at 6 months of age and 19.9% at 9 months of age (genotype effect $P < 0.0001$, age effect $P < 0.0001$, interaction $P < 0.0001$) (Fig. 8C). Similarly striatal DARPP-32 expression was reduced by 6.8% at 6 months of age and 23.8% at 9 months of age (genotype effect $P < 0.0001$, age effect $P < 0.0001$, interaction $P < 0.0001$) (Fig. 8D). Significant reductions in striatal expression of DRD2 and DARPP-32 have been reported from 9 months of age in YAC128 mice, but were not apparent at 6 months of age (23,60). Although onset of these changes was earlier in Hu128/21 mice, the magnitude of reduction was lower than that reported in YAC128 mice. These variations may be due to the use of different qPCR systems (TaqMan for YAC128 vs. Universal Probes for Hu128/21). Similar to what has been reported for YAC128 mice (60), a modest but significant 10.5% reduction in cannabinoid receptor 1 (CNR1) was observed in Hu128/21 striata at 9 months of age (genotype effect $P < 0.0001$, age effect $P < 0.0001$, interaction $P < 0.0001$) (Fig. 8E). Taken together these data demonstrate that Hu128/21 mice are an appropriate model for investigation of HD-like striatal gene expression changes.

Hu128/21 mice display elevated circulating IL-6

Elevated circulating pro-inflammatory cytokines have been reported in HD mutation carriers as much as 16 years before onset

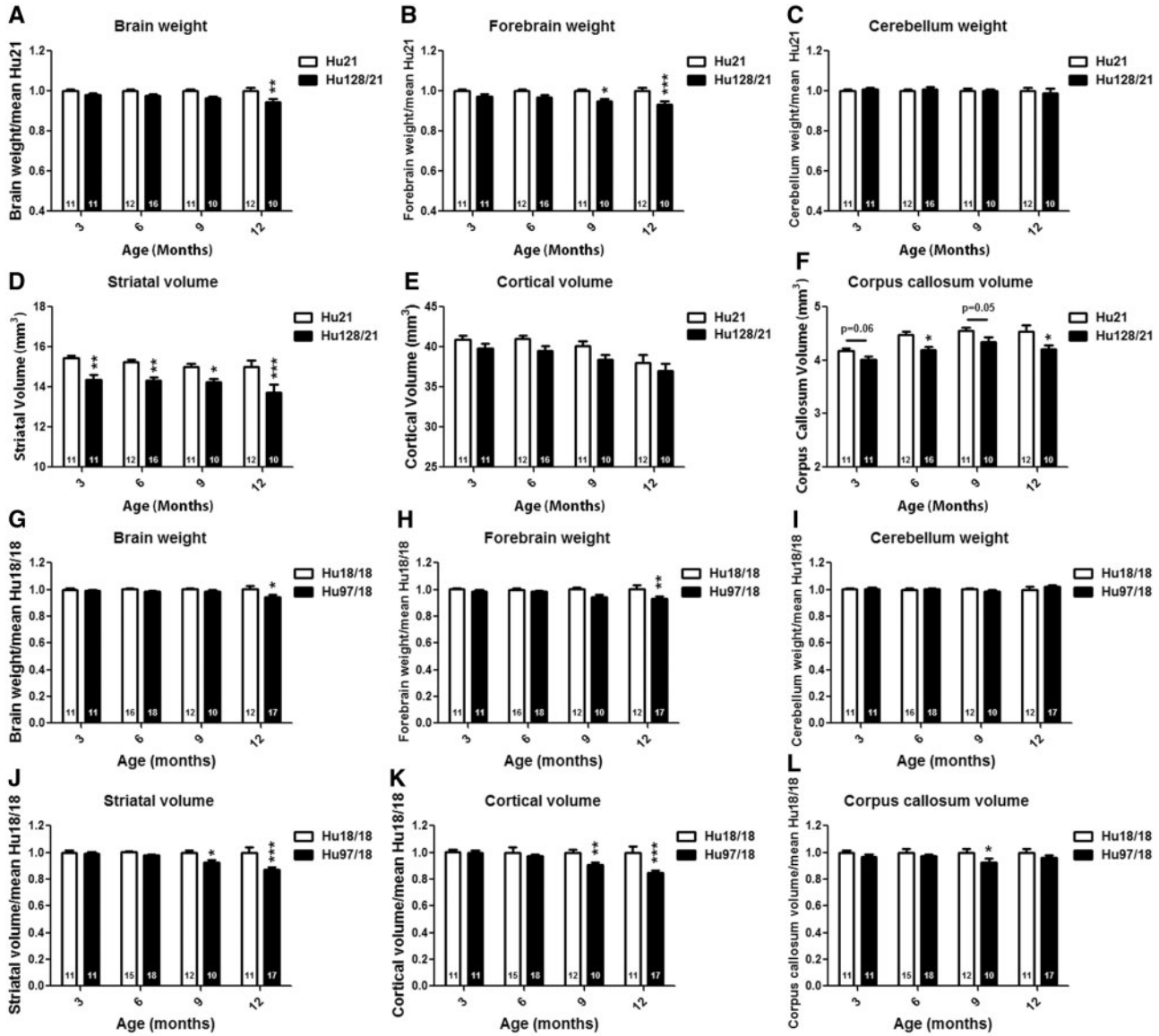

Figure 6. Hu128/21 mice display forebrain specific atrophy. Weights and structure volumes were assessed at 3, 6, 9 and 12 months of age. When compared with Hu21 control mice, Hu128/21 mice displayed reduced **(A)** total brain weight at 12 months of age and **(B)** forebrain weight from 9 months of age. **(C)** Cerebellum weight was not different between the genotypes. **(D)** Hu128/21 mice displayed striatal volume reduction from 3 months of age, the earliest time point evaluated. **(E)** There was a consistent trend toward reduced cortical volume at all ages, and a significant effect of genotype by two-way-ANOVA ($P = 0.0071$), but this failed to reach *post hoc* significance. **(F)** When compared with Hu21 brain, corpus callosum volume was significantly reduced in Hu128/21 brain at 6 and 12 months of age, with a trend toward reduction noted at 3 and 9 months of age. When compared with Hu18/18 control mice, Hu97/18 mice displayed reduced **(G)** total brain weight and **(H)** forebrain weight at 12 months of age. **(I)** Cerebellum weight was not different between the genotypes. Hu97/18 mice displayed significantly reduced **(J)** striatal volume and **(K)** cortical volume from 9 months of age. **(L)** When compared with Hu18/18 brain, corpus callosum volume was significantly reduced in Hu97/18 brain at 9 months of age, with a trend toward reduction noted at 12 months of age. Data for Hu97/18 line at 12 months of age were previously reported in (14) and is included here to allow direct comparison. *Different from Hu21 or Hu18/18 same age, $^{*}P < 0.05$, $^{**}P < 0.01$, $^{***}P < 0.001$.

of disease, and HD monocytes and macrophages exhibit hyperactive IL-6 release when stimulated (4). YAC128 mice recapitulate this pro-inflammatory immune state with elevated circulating IL-6 (61) and hyperactive release of IL-6 from stimulated macrophages and microglia that is directly attributable to cellular muHTT (4,62). Serum IL-6 was evaluated at 9 or 12 months of age by Meso Scale Discovery assay. When compared with Hu21 littermates, Hu128/21 mice were found to have significantly elevated circulating IL-6 at 12 months of age with a trend toward elevation noted at 9 months of age (genotype effect $P = 0.0094$, age effect $P = 0.1630$, interaction $P = 0.1630$) (Fig. 8F).

Allele-specific silencing of muHTT in Hu128/21 mice

We have previously shown that SNP rs7685686_G is targetable in neurons from YAC128 mice (18). However, we were not able to evaluate true allele-specificity because there is no homology between *Hdh* and human HTT at this intronic location. As a proof of concept for preclinical therapeutic development, Hu128/21 mice were used to screen ASOs for allele-specific silencing of muHTT by targeting SNP rs7685686_G, a polymorphism linked to HD in populations of East Asian descent and in a minority of patients in other ethnic groups. ASO designs were based on previous data targeting the rs7685686_A allele. To limit

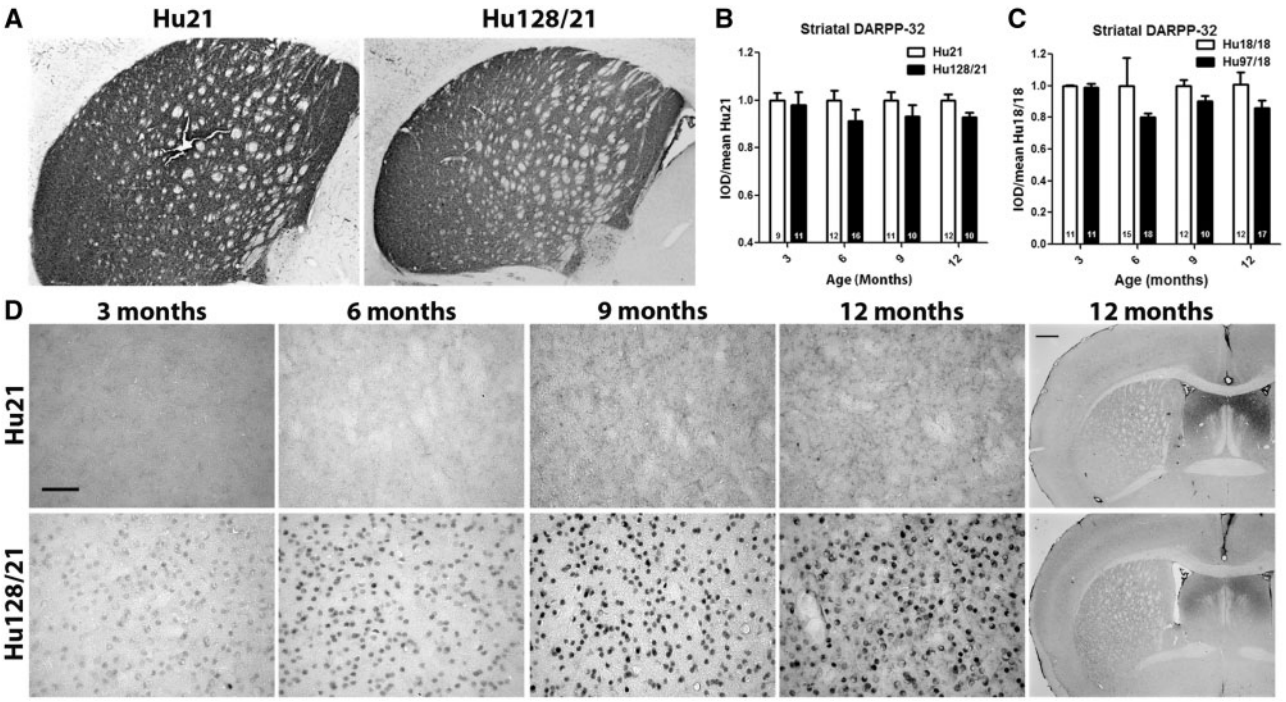

Figure 7. Hu128/21 display HD-like histological changes in the brain. **(A,B)** DARPP-32 immunoreactivity was assessed at 3, 6, 9 or 12 months of age by integrated optical density. (A) representative mid-striatal micrographs of Hu21 and Hu128/21 DARPP-32 stained brains at 12 months of age. (B) When compared with Hu21 controls, Hu128/21 mice display reduced striatal DARPP-32 (genotype effect $P = 0.0456$). This difference failed to reach *post hoc* significance at any age, but a trend toward reduction was noted at 6, 9 and 12 months of age. **(C)** When compared with Hu18/18 controls, Hu97/18 mice display reduced striatal DARPP-32 (genotype effect $P = 0.0135$). This difference failed to reach *post hoc* significance at any age, but a trend toward reduction was noted at 6, 9 and 12 months of age. Data for Hu97/18 line at 12 months of age was previously reported in (14) and is included here to allow direct comparison. **(D)** Hu128/21 mice display progressive deposition of striatal EM48 positive muHTT inclusions. Diffuse nuclear staining is apparent by 3 months of age and becomes progressively more intense with age. By 9 months of age, robust striatal inclusions are present. Inclusion deposition was also noted in cortex. Scale bars = 50 μm high magnification images and 500 μm low magnification images.

undesirable RNase H cleavage events the gap region was shortened to eight or seven nucleotides (X1, X2, X5 and X7) (20) or modified with nucleotide analogs at sensitive positions in the gap region (X3, X4 and X8) (63). Furthermore phosphodiester linkages were incorporated into the wings to modulate tolerability and distribution (X6 and X9).

ASOs were evaluated in a single dose *in vivo* screen in Hu128/21 brain. 300 μg of ASO was delivered by bolus injection to the right lateral ventricle. Allelic HTT protein was quantified 4 weeks later in anterior forebrain by allelic separation immunoblotting (Fig. 9). ASOs X1, X2, X3, X6 and X8 were found to be sufficiently potent, each inducing greater than 60% muHTT suppression (Table 1). ASOs X1, X3 and X8 were found to be the most selective, inducing only negligible reduction of wtHTT protein. ASO X6 failed to meet selectivity criteria, inducing a significant mean 24.6% suppression of wtHTT (Table 1). ASOs that met the potency criteria for this single dose screen were next evaluated in a dose response study in primary Hu128/21 neurons.

Primary Hu128/21 neurons were treated with bath applied ASO on day two in culture with ASO concentrations ranging from 4 to 1000 nM and evaluated 6 days post-treatment by allelic separation immunoblotting. The protein level of the two HTT alleles was normalized to calnexin loading control and then to the same allele from untreated neurons on the same membrane, and dose–response curves were generated (Fig. 10). HTT KD at each dose was evaluated by two-way ANOVA and preferential suppression of muHTT was found from 16 nM for ASOs X1, X2 and X3 and from 250 nM for ASOs X6 and X8. All ASOs were found to be sufficiently potent, reducing muHTT by 60–92% at 1000 nM with limited reduction of wtHTT protein (13–39%). Similar to the *in vivo* screen, ASO X6 was the most potent ASO and the least selective, significantly reducing wtHTT by 39%. ASO IC_{50} values were calculated using non-linear regression for each allele. All ASOs had IC_{50} values in the nanomolar range of 30–286 nM for muHTT KD, which is comparable to our previous study of ASOs targeting the other allele at this SNP (rs7685686_A) (18). Because <50% reduction of wtHTT was seen at the highest ASO concentration tested, it was not possible to calculate IC_{50} values for wtHTT. To account for this, selectivity was assessed by dividing the highest concentration (1000 nM) by the IC_{50} value for muHTT (18). Selectivity ranged from 4- to more than 29-fold (Table 1). ASOs X3 and X6 showed the greatest selectivity. However, it must be noted that this method of assessing selectivity is dependent on ASO potency and the high selectivity value of X6 despite significant KD of wtHTT is related to its higher potency rather than true higher selectivity of X6 than other ASOs evaluated.

Based on screen and dose response results, ASO X3 was identified as a lead candidate for allele-specific suppression of muHTT on C haplogroup.

Discussion

We have generated a novel humanized mouse model of HD, Hu128/21, to be used as a companion model to the existing Hu97/18 line. Hu128/21 mice derive muHTT from the YAC128 transgene and have similar wt and muHTT levels as the parental YAC128 line, indicating that variety and severity of HD-like phenotypes should be similar in the two lines. We found this to be true. The vast majority of evaluated HD-like phenotypes

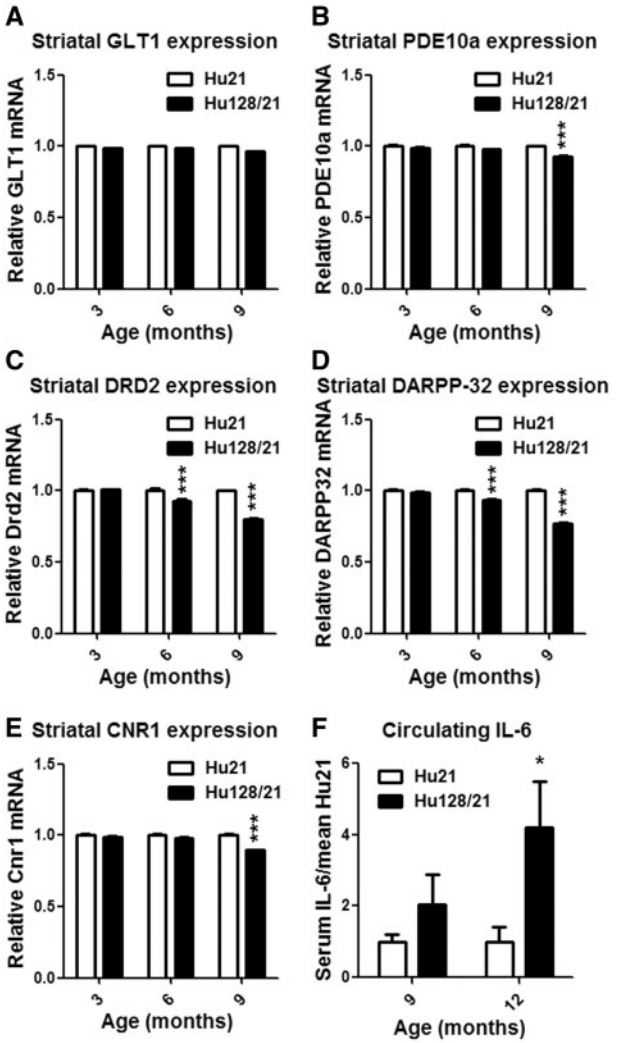

Figure 8. Hu128/21 mice display HD-like striatal gene expression changes and increased circulating IL-6. **(A–E)** Striatal gene expression was assessed through qRT-PCR at the indicated ages. (A) There was no effect of genotype on GLT1 expression. (B) Hu128/21 mice displayed a modest but significant reduction in striatal PDE10a expression at 9 months of age. (C, D) D2 dopamine receptor and DARPP-32 expression was progressively reduced in Hu128/21 striata from 6 months of age. (E) A modest but significant reduction in striatal CNR1 expression was noted in 9-month old Hu128/21 mice. **(F)** Serum IL-6 was quantified by MSD at the indicated ages. A trend toward increased circulating IL-6 was noted at 9 months of age with a significant increase at 12 months of age. *Different from Hu21 same age, $^{*}P < 0.05$, $^{**}P < 0.01$, $^{***}P < 0.001$.

previously validated in YAC128 mice were also apparent in Hu128/21 mice (Table 2).

The exception to this is cortical volume loss, for which YAC128 mice display a significant reduction at 12 months of age and Hu128/21 mice display a significant effect of genotype, but atrophy did not reach significance by *post hoc* analysis at 12 months of age, which was the latest time point evaluated. Additionally, Hu128/21 mice did not have a genotypic difference in climbing performance from Hu21 control mice. This was due to progressive deficits in the control Hu21 line rather than improved performance of Hu128/21 mice compared with YAC128 mice. Therefore, this does not result from the absence of an HD-like phenotype in Hu128/21 mice, but rather the confounding factors present in both the HD and control lines, such as weight gain and loss of endogenous mouse wtHtt.

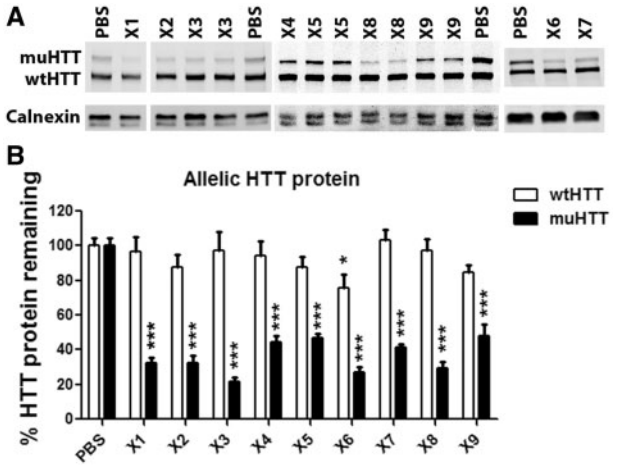

Figure 9. Single dose screen of C HTT haplogroup ASOs in Hu128/21 brain. 300 μg of ASO was delivered by unilateral ICV bolus injection to 6-week-old Hu128/21 mice. Four weeks later protein was isolated from a 2 mm coronal section from each hemisphere and evaluated for HTT protein by allelic separation immunoblotting. HTT levels were normalized to calnexin from the same sample as a loading control and then to the same allele from PBS injected animals on the same membrane. **(A)** Representative blot images. **(B)** Quantification of both hemispheres from an N of four animals per ASO. *Different from same allele PBS-treated animals, $^{*}P < 0.05$, $^{***}P < 0.001$.

Phenotypic age of onset was similar in YAC128 and Hu128/21 mice. However, a number of phenotypes were accelerated in the humanized model, including testicular degeneration, accelerating rotarod deficits, and corpus callosum atrophy. Acceleration of certain phenotypes could be related to the inability of human wtHTT to fully compensate for the loss of mouse endogenous wtHtt. Conversely, while the onset of forebrain atrophy is the same in YAC128 and Hu128/21 mice, whole brain atrophy has been reported at 9 months of age in YAC128 mice (12) and was not apparent in Hu128/21 mice until 12 months of age. Despite these slight variations in onset, the variety and severity of HD-like phenotypes were found to be similar in YAC128 and Hu128/21 mice. This is useful because the YAC128 mouse has been extensively characterized in over 130 Pubmed articles. Our data suggests that the vast amount of knowledge about the YAC128 model is likely applicable to the Hu128/21 model alleviating the need for extensive characterization of further endpoints prior to preclinical studies.

Variety and severity of HD-like phenotypes were also compared with Hu97/18 mice (Table 2). Many phenotypes were found to be similar with similar onset, including body weight gain, rotarod training deficits, anxiety-like behavior, depressive-like behavior and whole brain atrophy. Some phenotypes were accelerated in Hu128/21 mice compared with Hu97/18 mice, including accelerating rotarod deficits, object location and recognition learning deficits, forebrain atrophy and striatal and corpus callosum atrophy. Although other phenotypes were delayed in Hu128/21 mice as compared with Hu97/18 mice, including anxiety during elevated plus maze exploration and cortical atrophy. These variations are likely related to the differences in the BACHD and YAC128 muHTT transgenes.

It should also be noted that while both Hu97/18 and Hu128/21 mice display a progressive decline in motor performance, these models are not ideal for motor testing. The weight gain in the control humanized lines, Hu18/18 and Hu21 leads to progressive motor deficits that confound evaluation of muHTT specific effects. Some HD-like phenotypes were apparent in

Table 1. Summary of ASOs

ASO	Sequence/Design	*In vivo* screen		Neuronal dose response		
		%KD		IC50 (nM)		Fold selectivity
		wtHTT	muHTT	wtHTT	muHTT	
X1	ATAAATTGCCATCACC	3.4	67.6	>1000	74	>13.5
X2	TAAATTGCCATCACC	12.4	67.8	>1000	246	>4.1
X3	ATAAA$_{s2}$TTGCCATCACCA	2.9	78.4	>1000	34	>29.4
X4	TAAATTGCCATCACC	5.6	55.4			
X5	TAAATTGCCATCACC	12.4	52.8			
X6	ATTGCCATCACC_oA_oGA	24.6	72.9	840	30	28.0
X7	TAAATTGCCATCACCA	-3.2	58.2			
X8	ATAAATTGCCATCACCA	3	70.4	>1000	286.0	>3.5
X9	TA_oA_oATTGCCATCAC_oC_oAG	15.1	52.2			

Black-PS, MOE, cEt, 2-thio T, $_o$-phosphodiester linkage, Target SNP is underlined.

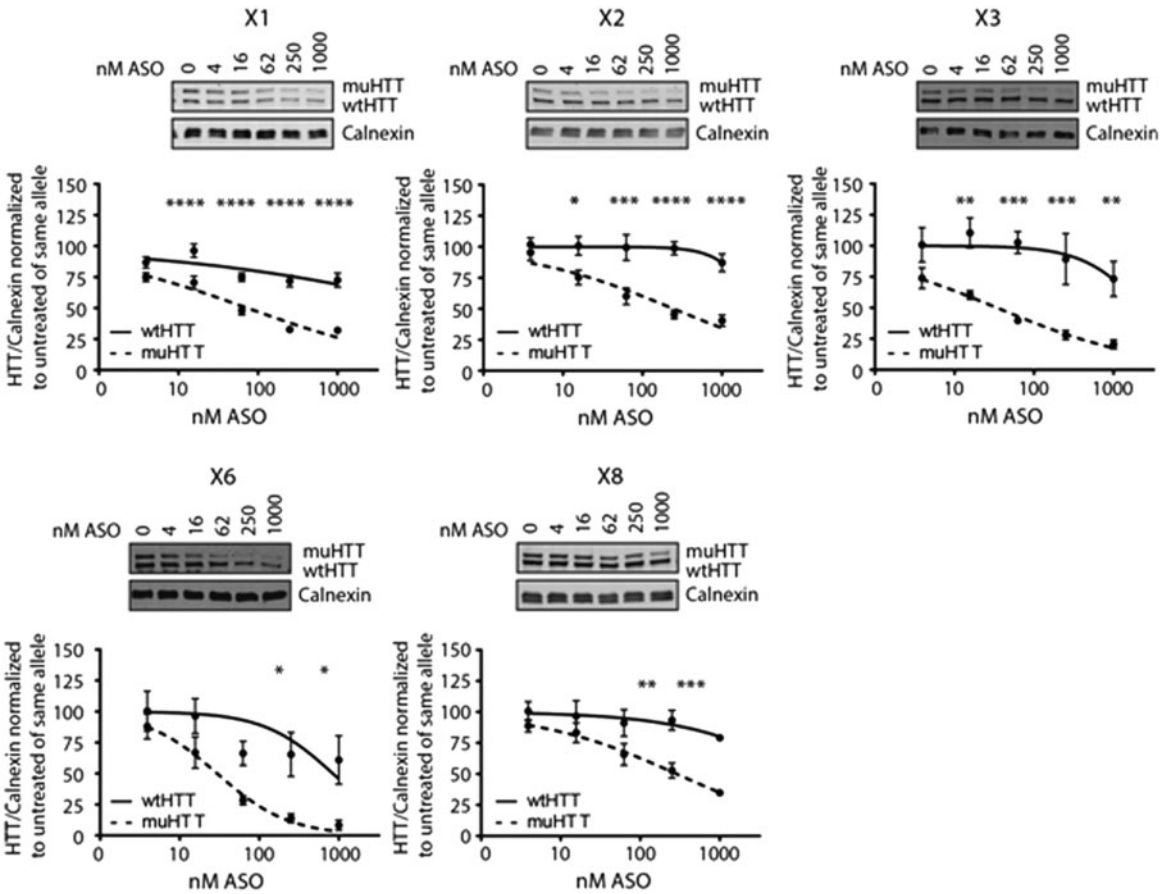

Figure 10. Dose response of C HTT haplogroup ASOs in primary Hu128/21 neurons. Primary Hu128/21 neurons were treated with the 5 most potent ASOs (>60%KD *in vivo*) at 4–1000 nM for 6 days. HTT KD was evaluated by allelic separation immunoblotting. Each HTT allele was normalized to the loading control calnexin and then to the same allele for the untreated sample. Representative images are shown for each ASO. Number of 4–12 per data point. Data are presented as mean ± SEM. Two-way ANOVA with Bonferroni *post hoc* test was performed. *Different from same allele untreated neurons, *$P < 0.05$, **$P < 0.01$, ***$P < 0.001$ and ****$P < 0.0001$.

Table 2. Comparison of onset of HD-like phenotypes in YAC128, Hu97/18 and Hu128/21 mouse lines

	YAC128	Hu97/18	Hu128/21
Transgene			
muHTT haplogroup	C	A	C
100% homology to h HTT	Yes	No	Yes
Pathology			
Body weight increase	2 months (27)	4 months (14)	4 months
Testicular degeneration	12 months (29)	ns	9 months
Whole brain atrophy	9 months (12)	12 months (14)	12 months
Forebrain atrophy	9 months (28)	12 months (14)	9 months
Striatal loss	3 months (41)	9 months	3 months[a]
Cortical loss	12 months (12)	9 months	ns
Corpus Callosum loss	12 months (28)	9 months	6 months
Cerebellum loss	None (12)	None (14)	None
Behaviour			
Rotarod training	2 months (31)	2 months (14)	2 months
Rotarod	4 months (45)	4 months (14)	2 months[a]
Climbing	6 months (28)	2 months[a] (14)	None
Exploratory activity	Normal (28)	Normal (14)	Normal
Open field anxiety	6 months[a] (33)	3 months[a] (14)	3 months[a]
Plus maze anxiety	8 months (28)	6 months (14)	9 months
Forced swim depression	3 months[a] (36)	3 months	3 months[a]
Spontaneous alternation	4 months[a] (28)	Normal	4 months[a]
Object location	6 months[a] (33)	6 months (14)	3 months[a]
Object recognition	6 months[a] (33)	9 months (14)	6 months
Transcript and protein levels			
EM48 positive inclusions	12 months[a] (12)	ND	9 months
DARPP-32 loss-protein	12 months[a] (45)	ND	6 months[a]
DARPP-32 loss-mRNA	9 months (60)	ND	6 months
Cnr1 loss-mRNA	9 months (60)	ND	9 months
GLT1 loss-mRNA	None (59)	ND	None
PDE10a loss-mRNA	ND	ND	9 months
Drd2 loss-mRNA	9 months (60)	ND	6 months
Elevated circulating IL-6	12 months (61)	ND	12 months

ND, not determined; ns, not significant (trend).

[a]Earliest time point evaluated.

Hu128/21 mice but not in Hu97/18 mice, including testicular degeneration and spontaneous alternation deficits. This is consistent with previous reports of HD-like phenotypes apparent in YAC128 mice that are absent in BACHD mice (23). Phenotypes previously noted to be absent in BACHD mice (23) were not evaluated in Hu97/18 mice. Hu97/18 muHTT is derived from the BACHD transgene at a reduced expression level, and phenotypic severity is decreased or delayed in Hu97/18 mice compared with BACHD mice (14). Thus, Hu97/18 mice would not be expected to display phenotypes that are absent in BACHD mice. The Hu128/21 mouse provides a humanized mouse model of HD for studies of these phenotypes that could not previously be addressed in Hu97/18 mice, including some striatal gene expression changes, robust muHTT aggregation and testicular degeneration.

Additionally, unlike the BACHD transgene, which carries a floxed, synthetic exon 1 sequence with 31 point mutations outside of the CAG tract region, exon 1 of the YAC128 and BAC21 transgene sequences shares 100% homology with the human HTT reference sequence. This means that therapeutics targeting human HTT exon 1 at the DNA or transcript level can be evaluated in Hu128/21 mice, which is not possible in Hu97/18 mice. Moreover, the CAG tract of the YAC128 transgene is less interrupted, and contains 80 contiguous CAG repeats compared with only two contiguous CAGs in any portion of the BACHD CAG tract (23). Thus, the Hu128/21 model can be used for studies of human HTT requiring contiguous CAG repeats that would not be possible in Hu97/18 mice, such as studies of RAN translation products or preclinical evaluation of experimental therapeutics targeting expanded CAG.

Finally, Hu128/21 mice have inverse HTT haplogroup alleles of Hu97/18 mice. Hu97/18 mice are an appropriate model for development of experimental therapeutics targeting muHTT with A haplogroup alleles, while Hu128/21 mice are an appropriate model for preclinical development of experimental therapeutics targeting muHTT with C haplogroup alleles. Thus, the generation of the Hu128/21 line greatly increases the proportion of the HD population for which a genetically relevant mouse model is available for the development of personalized gene silencing therapeutics. HTT haplogroup C is most frequently associated with CAG tract expansion in HD populations of East Asian descent (21). Additionally, 43% of Black South African HD mutations, and between 3.2 and 4.5% of HD mutations in patients of European ancestry, occur on the HTT haplogroup C (17,22). These patients would not benefit from allele-specific therapy targeted to the most common HD haplotypes in patients of European ancestry, and therefore represent a genetically distinct group for personalized allele-specific therapy targeting the C haplogroup (17,18). Gene silencing reagents targeting both alleles of rs7685686, or any other SNP distinguishing the A and C haplogroups, could also offer the possibility of allele-specific

treatment for approximately half of HD patients from diverse ethnic origins, coupled with non-specific silencing for all remaining patients (18).

In this proof of concept study, Hu128/21 mice were used to screen and evaluate ASOs targeting a HTT haplogroup C polymorphism. A panel of nine ASOs (X1–X9) was designed for high potency and selectivity using knowledge gained from previous studies (10,18,20,63). ASOs were evaluated both in a single dose *in vivo* screen and in a dose response in primary cultured neurons. All ASOs showed activity against muHTT with five of nine showing high potency with >60% muHTT suppression. High selectivity, as noted by no significant suppression of wtHTT and IC_{50} for wtHTT > 1000 nM, was observed for eight of the nine ASOs. ASO X3 was identified as a lead ASO for allele-specific suppression of C haplogroup HTT, validating the Hu128/21 model as a tool for preclinical therapeutic evaluations.

The Hu128/21 mouse model of HD recapitulates a wide variety of HD-like phenotypes, including psychiatric and cognitive behavioral changes as well as biochemical, neuropathological and gene expression changes. Hu128/21 mice display HD-like phenotypes not apparent in Hu97/18 mice, allowing for their study in a humanized HD mouse for the first time. Additionally, the Hu128/21 mouse has novel applications in preclinical development of experimental therapeutics targeting human HTT exon 1, human HTT with expanded CAG, and C haplogroup HTT polymorphisms.

Materials and Methods

Mice and breeding

Mice were maintained under a 12-h light:12-h dark cycle in a clean facility and given free access to food and water. Experiments were performed with the approval of the animal care committee of the University of British Columbia (UBC) or the Institute Animal Care and Use Committee of the University of Los Angeles at California. Cohorts of mice used for characterization of the Hu128/21 line consisted of approximately equal numbers of males and females and Hu21 and Hu128/21 genotypes.

For generation of BAC21 mice, BAC DNA was purified from human Huntingtin BAC clone (RP11-866L6) using our established method (11). BAC DNA was linearized with PI-SceI and microinjected into fertilized eggs from FVB/NJ mice prior to transferring into pseudo-pregnant female mice. Transgenic founder mice were confirmed by PCR genotyping and CAG repeat length was sized by Laragen (Los Angeles, CA). The expression of full-length human huntingtin in the BAC21 mice was confirmed by Western blot analysis.

BAC21 mice were imported to UBC and intercrossed with *Hdh*+/− mice (64) to generate BAC21 mice on the *Hdh*−/− background (Hu21). YAC128 mice (12) on the *Hdh*−/− (Hu128) background were generated in a similar way. Male Hu21 and female Hu128 mice were then intercrossed to generate Hu21, Hu128 and Hu128/21 mice. Genotyping was performed using CAG tract spanning PCR with the following reagents; 10% DMSO, 0.4 μM each primer, 1× BSA, 2.2 mM dNTPs, 1× GB buffer (5× GB buffer: 3.35 ml 1M TRIS, 35 μl β-mercaptoethanol, 830 μl 1M $(NH4)_2SO4$, 100 μl 1M $MgCl_2$, dH_2O to 10 ml), and 0.63 U Taq polymerase (Roche), the following primer sequences; CAG3_F: 5′ ATT GCC CCG GTG CTG AGC G 3′, CAG3_R: 5′ GCG GGC CCA AAC TCA CGG TC 3′ and the following reaction conditions; 94°C 30 s, 34×(94°C 30 s, 61°C 30 s, 72°C 90 s), 72°C 10 min. Intergenerational CAG tract length was compared with confirm stability of the YAC128 muHTT CAG tract, which has been previously reported in (65). Crosses of female Hu21 and male Hu128 mice produced no litters indicating sterility of one of these breeder types. Additionally, litter size for the Hu128/21 line is small because the cross generates ∼25% *Hdh*−/− mice, which are resorbed as embryos (64), resulting in ∼75% live births.

Exon 1 sequencing

Genomic DNA was extracted from BACHD or BAC21 tail biopsies using the DNeasy Blood and Tissue Kit (Qiagen). For BACHD, 100 ng of genomic DNA and KODXtreme Hot Start DNA Polymerase (Novagen) were used in a total reaction volume of 50 μl for the amplification of exon 1. The primers used were LKH5 (5′ TGGGTTGCTGGGTCACTCTGTC 3′) and LKH1 (5′ CCCATTC ATTGCCCCGGTGCTG 3′). The cycling conditions were: (i) 94°C for 3 min, (ii) 30 cycles of 94°C for 30 s, 60°C for 30 s and 72°C for 1 min and (iii) 72°C for 10 min. For BAC21, Platinum Pfx polymerase with 1 mM $MgSO_4$ and PCR enhancer solution (Thermofisher) were used for the amplification of exon 1. The primers used were HTT_CAG_3F (5′ ATTGCCCCGGTGCTGAGCG 3′) and HTT_CAG_3R (5′ GCGGGCCCAAACTCACGGTC 3′). The cycling conditions were: (i) 94°C for 3 min, (ii) 35 cycles of 94°C for 30 s, 61°C for 45 s and 72°C for 1 min and (iii) 72°C for 7 min. The resultant amplicons were separated and visualized using agarose gel electrophoresis. The corresponding band was excised and the amplicon was extracted using QIAquick Gel Extraction Kit (Qiagen). For BACHD sequencing, the fragment was cloned into pBLUNT using Zero Blunt PCR Cloning Kit (Thermo Fisher Scientific) according to the manufacturer's instructions. The cloned plasmids were sequenced using the universal M13F primer. For BAC21 sequencing, the gel purified amplicon was directly sequenced using the HTT_CAG_3F and R primers.

HTT levels

Four-month old Hu128/21, Hu128, Hu21, YAC128, BAC21 and FVB mice were killed with an overdose of 2.5% Avertin IP. Brains were removed, chilled briefly on ice and microdissected by region. Left cortices from four mice per genotype were used for HTT quantitation by allelic separation immunoblotting as previously described in (14). Briefly, 40 μg of total protein was resolved on 10% low-BIS acrylamide gels (9), transferred to 0.45 μm nitrocellulose and blotted for human HTT (MAB2168, Millipore) or total HTT (MAB2166, Millipore) and calnexin (Sigma C4731) loading control. Primary antibodies were detected with IR dye 800CW goat anti-mouse (Rockland 610-131-007) and AlexaFluor 680 goat anti-rabbit (Molecular Probes A21076)-labeled secondary antibodies, and the LiCor Odyssey Infrared Imaging system. Expression intensities were quantified with LiCor Image Studio Lite software, and HTT intensities were normalized to calnexin loading control.

Behavior testing

Longitudinal accelerating rotarod was performed at 2-month intervals from 2 to 12 months of age as previously described in (14). Briefly, 2-month old mice were trained over three 120 s trials per day for 3 days on an 18 rpm fixed speed rotarod. Mice that fell were returned immediately to the rod. Mean latency to the first fall and mean falls for the three trials were scored. Mice were tested over three 300 s trials on an accelerating rotarod (5–40 rpm). Mean latency to fall for the three trials was

scored. Body weight was also scored on the day of rotarod testing prior to the test.

Longitudinal climbing was performed at 2-month intervals from 2 to 12 months of age as previously described in (14). Briefly, mice were recorded by video camera during a 5 min exploration of an inverted wire pencil holder on the bench top. Latency to begin climbing (all 4 ft off of the bench top), number of climbing events and total time spent climbing were scored.

Open field exploration and object learning were performed at 3, 6 or 9 months of age (in different cohorts) as previously described in (14). Briefly, mice were placed in a 50 × 50 cm open top box under bright lighting and recorded via ceiling-mounted video camera during a 10 min exploration. Distance traveled and time spent in the center of the field were scored using Ethovision XT 7 animal tracking software (Noldus) as measures of activity and anxiety, respectively. Data for any mouse with mean velocity under 2 cm/s were excluded for lack of exploration. After a 5-min inter-trial interval (ITI), mice were returned to the box, now containing two objects in the upper corners of the box ∼7 cm from the sides. After a 5-min exploration, mice were given a 5-min ITI during which the object on the right was moved to the lower corner. Mice were given another 5-min exploration. Investigations to the target object on the right were scored as a measure of spatial learning. On the following day mice were returned to the box for a 5-min acclimation, given a 5-min ITI, and then allowed to explore the box for 5 min with the same two objects in their original positions. After a 5-min ITI, the object on the right was replaced with a novel object, and the mice were given another 5-min exploration. Investigations to the target objet on the right were scored as a measure of object recognition. Data for any mouse that failed to investigate both objects were excluded.

Elevated plus maze exploration was performed at 3, 6 or 9 months of age (in different cohorts) as previously described in (14). Briefly, mice were placed in the center of an elevated plus maze, and exploration was recorded during a 5-min trial by a ceiling-mounted video camera. Total distance traveled was scored as a measure of exploratory activity and time spent in the open arms and number of head dips off the edge of the open arms was scored as a measure of anxiety. Data for any mouse with mean velocity of <2 cm/s were excluded for lack of exploration.

A modified Porsolt forced swim test was performed at 3, 6, 9 or 12 months of age (in different cohorts) as previously described in (36). Briefly, mice were placed in a transparent cylinder filled with room temperature water for 6 min and recorded with a video camera. Time spent immobile was scored for the final 5 min of the trial as a measure of depression. Due to the stressful nature of this test it was the final behavior test performed for each group of mice.

Spontaneous alternation was performed at 4 months of age as previously described in (39). Briefly, mice were placed at the base of a T maze and allowed to choose a goal arm. A barrier was lowered to prevent exit from the goal arm during a 1-min exploration. Mice were then immediately placed at the base of the T and once again allowed to choose a goal arm. The percentage of mice alternating (entering the previously unexplored goal arm) was scored as a measure of spatial learning.

Neuropathology and brain histology

Mice were anesthetized with 2.5% Avertin IP followed by transcardiac perfusion with phosphate buffered saline (PBS) and 4% paraformaldehyde (PFA). Brains and testes were removed and post-fixed in 4% PFA in PBS for 24 h at 4°C. The following day testes were weighed and brains were cryoprotected in 30% sucrose with 0.01% sodium azide. Once equilibrated, brains were weighed whole, divided into forebrain and cerebellum and weighed again. Forebrains were then frozen on dry ice, mounted in Tissue-TEK O.C.T. embedding compound (Sakura) and cut via cryostat (Leica CM3050S) into a series of 25 μm coronal sections free-floating in PBS with 0.01% sodium azide.

Stereological volumetric analysis was performed as in (14). Briefly, a series of sections spaced 200 μm apart and spanning the striatum was stained for NeuN (1:1000, Millipore) using biotinylated anti-mouse secondary antibody (1:1000, Vector Laboratories), the ABC Elite Kit (Vector) to amplify signal, and 3,3′-diaminobenzidine (DAB) (Thermo Scientific) detection. Structures were traced using Stereo Investigator software (MBF Bioscience) and volumes determined using the Cavalieri principle.

Striatal immunohistochemistry was performed as in (14). Briefly, a series of 4 mid-striatal sections were stained for DARPP-32 (1:500, R&D Systems) or HTT (EM48 1:100, Millipore) using biotinylated goat anti-rat (1:1000, Vector) or goat anti-mouse (1:500, Vector) secondary antibodies, the ABC Elite Kit, and DAB detection. Sections were imaged with a 5× or 40× objective (Zeiss) using a Zeiss Axioplan 2 microscope and Coolsnap HQ Digital CCD camera (Photometrics, Tucson, AZ, USA) and MetaMorph software (Molecular Devices). Staining intensity and integrated optical density of DARPP-32 were determined using ImageJ software. Values were normalized to the mean value for Hu21 mice from the same age and cohort.

Striatal gene expression

Striatal expression of HD-associated genes was evaluated at 3, 6 or 9 months of age as previously described in (66,67). Briefly, total RNA was isolated using Qiagen's RNeasy kit and reverse transcribed to cDNA using SuperScript III reverse transcriptase (Thermo Fisher). cDNA was amplified using FastStart Universal Probe Master (Rox)(Roche), Universal Probe Library probe (Roche), and gene-specific primer, using an ABI 7500 Fast Real-Time PCR System (Applied Biosystems). The mean of the Ct values from triplicate wells was assessed for each sample. Relative quantity of target genes; Drd2, DARPP-32, Cnr1, PDE10a and GLT1, was normalized to the mean quantity for three housekeeping genes; ATP5b, EIF4A2 and Ubc, for which no genotype specific effects were observed. Values were then normalized to the mean value for Hu21 mice of the same age.

Circulating IL-6

Blood was collected by cardiac puncture and plasma isolated at 9 or 12 months of age (in different cohorts). 25 μl of plasma was used to evaluate IL-6 level using the V-PLEX Plus Mouse IL-6 Kit (MesoScale Discoveries) according to the manufacturer's instructions. Samples were run in duplicate and the mean value for each mouse was normalized to the mean value for Hu21 mice at each age.

ASO synthesis

ASOs were synthesized on a 40 μmol scale using an AKTA synthesizer. ASO was synthesized on a polystyrene NittoPhase unylinker support. Protected nucleosides were incorporated

using standard solid-phase phosphoramidite chemistry and purified using ion-exchange HPLC as previously described in (20). ASO purity and identity was determined using liquid chromatography-coupled mass spectrometry.

In vivo ASO treatments

ASOs were evaluated for KD of wt and muHTT in Hu128/21 brain as previously described in (10). Briefly, 300 μg of ASO in 10 μl in sterile PBS was delivered by bolus injection to the right lateral ventricle using a Hamilton syringe with 26-gauge needle (Hamilton) at 0.3-mm anterior and 1-mm lateral to Bregma. The needle was punched through the skull and lowered to 3 mm below the surface. ASO was injected over 10 s, and the needle was left in place for 2 min before slow withdrawal. Four animals were treated with each ASO. Four weeks later mice were killed and brains were sectioned in a 1 mm coronal brain matrix (ASI Instruments). A section containing the second 2 mm was divided into right and left hemispheres and snap frozen for protein isolation. Total protein lysates from each 2 mm coronal hemisphere were evaluated for allelic HTT protein levels as above. HTT intensities were normalized to calnexin loading control and then to the mean value of the same allele from PBS injected animals on the same membrane to determine %KD.

Neuronal culture and ASO treatments

Brains were collected from embryos on day 15.5–16.5 of gestation and transferred to Hibernate E (Invitrogen) for 24 h. Gentoyping from tail biopsies was performed as earlier. Hu128/21 mixed striatal and cortical cultures were established as previously described in (18). Briefly, tissue was trypsinized for 8 min at 37°C and cells resuspended in complete culture media (Neurobasal media (NBM) containing 2% B27, 100 U/ml PS, and 0.5 mM L-Glutamine (Gibco)), and treated with DNAse I (153 U/ml) (Invitrogen). After trituration, 1.2×10^6 cells/well were seeded in poly-D-lysine coated 6-well plates in 2 ml of NBM+ and maintained in a humidified incubator at 37°C and 5% CO_2. On the second day *in vitro* (DIV) neurons were treated with ASO (0–1000 nM) in 200 μl fresh medium. Neurons were harvested at DIV 8 (6 days of treatment) by scraping in ice cold PBS. Cells were collected by centrifugation at 3500 g for 5 min at 4°C and pellets stored at −80°C until use. Pellets were lysed as in (18) and 25–40 μg of total protein was used to evaluate HTT protein levels by allelic separation immunoblotting as above.

Statistical analysis

Mice exhibiting a reactive phenotype as determined by abnormal brain morphology (enlarged triangular forebrain and total brain weight over 500 mg) were excluded from analysis. Data are expressed as mean ± SEM unless otherwise noted. Data from males and females were compared and combined when not significantly different. Data presented are from combined males and females unless otherwise noted. Analyses were performed using one- or two-way-ANOVA and Bonferroni *post hoc* tests unless otherwise noted. Differences were considered statistically significant for $P < 0.05$. For non-longitudinal tests n is reported on the bar graphs. IC_{50} curves were generated using non-linear regression with normalized response and a variable curve. Allele specificity was calculated by dividing the highest ASO concentration tested (1000 nM) by the IC_{50} for muHTT reduction and expressed as >fold change. Analyses were performed using GraphPad Prism V.5.

Supplementary Material

Supplementary Material is available at *HMG* online.

Acknowledgements

The authors thank Shaun Sanders for assistance optimizing HTT immunoblotting, Boguslaw Felczak, Qingwen Xia and Mark Wang for technical assistance and Mahsa Amirabbasi for administrative support.

Conflict of Interest statement M.E.O., H.B.K., E.E.S, and P.P.S. are employees of IONIS Pharmaceuticals. IONIS Pharmaceuticals synthesized and provided the ASOs used in this study, and supported work in the laboratory of M.R.H. M.R.H. is an employee of Teva Pharmaceuticals. No conflict of interest declared for all other authors.

Funding

This work was supported by grants from the Canadian Institutes of Health Research (CIHR) (MOP-84438) and the CHDI foundation to M.R.H and postdoctoral fellowships for A.L.S. and N.H.S. from CIHR and for A.L.S. from The Huntington Society of Canada, The Michael Smith Foundation for Health Research, and the Huntington's Disease Society of America. M.R.H. is a Killam University Professor and holds a Canada Research Chair. J.O. and M.A.P. are supported by funding from the Agency for Science Technology and Research (Singapore) and the National University of Singapore.

References

1. The Huntington's Disease Collaborative Research Group. (1993) A novel gene containing a trinucleotide repeat that is expanded and unstable on Huntington's disease chromosomes. *Cell*, **72**, 971–983.
2. Zuccato, C., Valenza, M. and Cattaneo, E. (2010) Molecular mechanisms and potential therapeutical targets in Huntington's disease. *Physiol. Rev.*, **90**, 905–981.
3. Ross, C.A. and Tabrizi, S.J. (2011) Huntington's disease: from molecular pathogenesis to clinical treatment. *Lancet Neurol.*, **10**, 83–98.
4. Bjorkqvist, M., Wild, E.J., Thiele, J., Silvestroni, A., Andre, R., Lahiri, N., Raibon, E., Lee, R.V., Benn, C.L., Soulet, D. *et al.* (2008) A novel pathogenic pathway of immune activation detectable before clinical onset in Huntington's disease. *J. Exp. Med.*, **205**, 1869–1877.
5. Ghosh, R. and Tabrizi, S. (2013) Clinical aspects of Huntington's disease. In Nguyen, H.H.P. and Cenci, M.A. (eds.), *Current Topics in Behavioral Neuroscience*. Springer, Berlin Heidelberg, pp. 1–29.
6. Petersen, A. and Bjorkqvist, M. (2006) Hypothalamic-endocrine aspects in Huntington's disease. *Eur. J. Neurosci.*, **24**, 961–967.
7. Zielonka, D., Mielcarek, M. and Landwehrmeyer, G.B. (2015) Update on Huntington's disease: Advances in care and emerging therapeutic options. *Parkinsonism Relat. Disord.*, **21**, 169–178.
8. Barnes, G., Duyao, M., Ambrose, C., McNeil, S., Persichetti, F., Srinidhi, J., Gusella, J. and MacDonald, M. (1994) Mouse

Huntington's disease gene homolog. *Somat. Cell Mol. Genet.*, **20**, 87–97.
9. Carroll, J.B., Warby, S.C., Southwell, A.L., Doty, C.N., Greenlee, S., Skotte, N., Hung, G., Bennett, C.F., Freier, S.M. and Hayden, M.R. (2011) Potent and selective antisense oligonucleotides targeting single-nucleotide polymorphisms in the Huntington disease gene/Allele-specific silencing of mutant huntingtin. *Mol. Ther.*, **19**, 2178–2185.
10. Southwell, A.L., Skotte, N.H., Kordasiewicz, H.B., Ostergaard, M.E., Watt, A.T., Carroll, J.B., Doty, C.N., Villanueva, E.B., Petoukhov, E., Vaid, K. *et al.* (2014) In vivo evaluation of candidate allele-specific mutant huntingtin gene silencing antisense oligonucleotides. *Mol. Ther.*, **22**, 2093–2106.
11. Gray, M., Shirasaki, D.I., Cepeda, C., André, V.M., Wilburn, B., Lu, X.H., Tao, J., Yamazaki, I., Li, S.H., Sun, Y.E. *et al.* (2008) Full-length human mutant huntingtin with a stable polyglutamine repeat can elicit progressive and selective neuropathogenesis in BACHD mice. *J. Neurosci.*, **28**, 6182–6195.
12. Slow, E.J., van Raamsdonk, J., Rogers, D., Coleman, S.H., Graham, R.K., Deng, Y., Oh, R., Bissada, N., Hossain, S.M., Yang, Y.Z. *et al.* (2003) Selective striatal neuronal loss in a YAC128 mouse model of Huntington disease. *Hum. Mol. Genet.*, **12**, 1555–1567.
13. Hodgson, J.G., Agopyan, N., Gutekunst, C.A., Leavitt, B.R., LePiane, F., Singaraja, R., Smith, D.J., Bissada, N., McCutcheon, K., Nasir, J. *et al.* (1999) A YAC mouse model for Huntington's disease with full-length mutant huntingtin, cytoplasmic toxicity, and selective striatal neurodegeneration. *Neuron*, **23**, 181–192.
14. Southwell, A.L., Warby, S.C., Carroll, J.B., Doty, C.N., Skotte, N.H., Zhang, W., Villanueva, E.B., Kovalik, V., Xie, Y., Pouladi, M.A. *et al.* (2013) A fully humanized transgenic mouse model of Huntington disease. *Hum. Mol. Genet.*, **22**, 18–34.
15. Kolodziejczyk, K., Parsons, M.P., Southwell, A.L., Hayden, M.R. and Raymond, L.A. (2014) Striatal synaptic dysfunction and hippocampal plasticity deficits in the Hu97/18 mouse model of Huntington disease. *PLoS One*, **9**, e94562.
16. Warby, S.C., Montpetit, A., Hayden, A.R., Carroll, J.B., Butland, S.L., Visscher, H., Collins, J.A., Semaka, A., Hudson, T.J. and Hayden, M.R. (2009) CAG expansion in the Huntington disease gene is associated with a specific and targetable predisposing haplogroup. *Am. J. Hum. Genet.*, **84**, 351–366.
17. Kay, C., Collins, J.A., Skotte, N.H., Southwell, A.L., Warby, S.C., Caron, N.S., Doty, C.N., Nguyen, B., Griguoli, A., Ross, C.J. *et al.* (2015) Huntingtin haplotypes provide prioritized target panels for allele-specific silencing in Huntington disease patients of European ancestry. *Mol. Ther.*, 1759–1771.
18. Skotte, N.H., Southwell, A.L., Ostergaard, M.E., Carroll, J.B., Warby, S.C., Doty, C.N., Petoukhov, E., Vaid, K., Kordasiewicz, H., Watt, A.T. *et al.* (2014) Allele-specific suppression of mutant huntingtin using antisense oligonucleotides: providing a therapeutic option for all Huntington disease patients. *PLoS One*, **9**, e107434.
19. Østergaard, M.E., Thomas, G., Koller, E., Southwell, A.L., Hayden, M.R. and Seth, P.P. (2015) Biophysical and biological characterization of hairpin and molecular beacon RNase H active antisense oligonucleotides. *ACS Chem. Biol.*, **10**, 1227–1233.
20. Østergaard, M.E., Southwell, A.L., Kordasiewicz, H., Watt, A.T., Skotte, N.H., Doty, C.N., Vaid, K., Villanueva, E.B., Swayze, E.E., Frank Bennett, C. *et al.* (2013) Rational design of antisense oligonucleotides targeting single nucleotide polymorphisms for potent and allele selective suppression of mutant Huntingtin in the CNS. *Nucleic Acids Res.*, **41**, 9634–9650.
21. Warby, S.C., Visscher, H., Collins, J.A., Doty, C.N., Carter, C., Butland, S.L., Hayden, A.R., Kanazawa, I., Ross, C.J. and Hayden, M.R. (2011) HTT haplotypes contribute to differences in Huntington disease prevalence between Europe and East Asia. *Eur. J. Hum. Genet.*, **19**, 561–566.
22. Baine, F.K., Kay, C., Ketelaar, M.E., Collins, J.A., Semaka, A., Doty, C.N., Krause, A., Jacquie Greenberg, L. and Hayden, M.R. (2013) Huntington disease in the South African population occurs on diverse and ethnically distinct genetic haplotypes. *Eur. J. Hum. Genet.*, **21**, 1120–1127.
23. Pouladi, M.A., Stanek, L.M., Xie, Y., Franciosi, S., Southwell, A.L., Deng, Y., Butland, S., Zhang, W., Cheng, S.H., Shihabuddin, L.S. *et al.* (2012) Marked differences in neurochemistry and aggregates despite similar behavioural and neuropathological features of Huntington disease in the full-length BACHD and YAC128 mice. *Hum. Mol. Genet.*, **21**, 2219–2232.
24. Banez-Coronel, M., Ayhan, F., Tarabochia, A.D., Zu, T., Perez, B.A., Tusi, S.K., Pletnikova, O., Borchelt, D.R., Ross, C.A., Margolis, R.L. *et al.* (2015) RAN translation in Huntington disease. *Neuron*, **88**, 667–677.
25. Miniarikova, J., Zanella, I., Huseinovic, A., van der Zon, T., Hanemaaijer, E., Martier, R., Koornneef, A., Southwell, A.L., Hayden, M.R., van Deventer, S.J. *et al.* (2016) Design, characterization, and lead selection of therapeutic miRNAs targeting huntingtin for development of gene therapy for Huntington's disease. *Mol. Ther. Nucleic Acids*, **5**, e297.
26. Graham, R.K., Slow, E.J., Deng, Y., Bissada, N., Lu, G., Pearson, J., Shehadeh, J., Leavitt, B.R., Raymond, L.A. and Hayden, M.R. (2006) Levels of mutant huntingtin influence the phenotypic severity of Huntington disease in YAC128 mouse models. *Neurobiol. Dis.*, **21**, 444–455.
27. Van Raamsdonk, J.M., Gibson, W.T., Pearson, J., Murphy, Z., Lu, G., Leavitt, B.R. and Hayden, M.R. (2006) Body weight is modulated by levels of full-length Huntingtin. *Hum. Mol. Genet.*, **15**, 1513–1523.
28. Southwell, A.L., Franciosi, S., Villanueva, E.B., Xie, Y., Winter, L.A., Veeraraghavan, J., Jonason, A., Felczak, B., Zhang, W., Kovalik, V. *et al.* (2015) Anti-semaphorin 4D immunotherapy ameliorates neuropathology and some cognitive impairment in the YAC128 mouse model of Huntington disease. *Neurobiol. Dis.*, **76**, 46–56.
29. Van Raamsdonk, J.M., Murphy, Z., Selva, D.M., Hamidizadeh, R., Pearson, J., Petersen, A., Bjorkqvist, M., Muir, C., Mackenzie, I.R., Hammond, G.L. *et al.* (2007) Testicular degeneration in Huntington disease. *Neurobiol. Dis.*, **26**, 512–520.
30. The Huntington Study Group. (1996) Unified Huntington's disease rating scale: reliability and consistency. *Mov. Disord.*, **11**, 136–142.
31. Van Raamsdonk, J.M., Pearson, J., Slow, E.J., Hossain, S.M., Leavitt, B.R. and Hayden, M.R. (2005) Cognitive dysfunction precedes neuropathology and motor abnormalities in the YAC128 mouse model of Huntington's disease. *J. Neurosci.*, **25**, 4169–4180.
32. E., van Duijn, M.D., E.M., Kingma, M.S.M.p. R.C. and van der Mast, M.D.P.D. (2007) Psychopathology in verified Huntington's disease gene carriers. *J. Neuropsychiatry Clin. Neurosci.*, **19**, 441–448.
33. Southwell, A.L., Ko, J. and Patterson, P.H. (2009) Intrabody gene therapy ameliorates motor, cognitive, and neuropathological symptoms in multiple mouse models of Huntington's disease. *J. Neurosci.*, **29**, 13589–13602.

34. Grote, H.E., Bull, N.D., Howard, M.L., Van Dellen, A., Blakemore, C., Bartlett, P.F. and Hannan, A.J. (2005) Cognitive disorders and neurogenesis deficits in Huntington's disease mice are rescued by fluoxetine. *Eur. J. Neurosci.*, **22**, 2081–2088.
35. Pang, T.Y.C., Du, X., Zajac, M.S., Howard, M.L. and Hannan, A.J. (2009) Altered serotonin receptor expression is associated with depression-related behavior in the R6/1 transgenic mouse model of Huntington's disease. *Hum. Mol. Genet.*, **18**, 753–766.
36. Pouladi, M.A., Graham, R.K., Karasinska, J.M., Xie, Y., Santos, R.D., Petersen, A. and Hayden, M.R. (2009) Prevention of depressive behaviour in the YAC128 mouse model of Huntington disease by mutation at residue 586 of huntingtin. *Brain*, **132**, 919–932.
37. Paulsen, J.S., Langbehn, D.R., Stout, J.C., Aylward, E., Ross, C.A., Nance, M., Guttman, M., Johnson, S., MacDonald, M., Beglinger, L.J. *et al.* (2008) Detection of Huntington's disease decades before diagnosis: the Predict-HD study. *J. Neurol. Neurosurg. Psychiatry*, **79**, 874–880.
38. Taketo, M., Schroeder, A., Mobraaten, L., Gunning, K., Hanten, G., Fox, R., Roderick, T., Stewart, C., Lilly, F. and Hansen, C. (1991) FVB/N: an inbred mouse strain preferable for transgenic analyses. *Proc. Natl. Acad. Sci. U. S. A.*, **88**, 2065.
39. Carroll, J., Southwell, A., Graham, R., Lerch, J., Ehrnhoefer, D., Cao, L.P., Zhang, W.N., Deng, Y., Bissada, N., Henkelman, R. *et al.* (2011) Mice lacking caspase-2 are protected from behavioral changes, but not pathology, in the YAC128 model of Huntington disease. *Mol. Neurodegener.*, **6**, 59.
40. Vonsattel, J.P., Keller, C. and Cortes Ramirez, E.P. (2011) Huntington's disease - neuropathology. *Handbook Clin. Neurol.*, **100**, 83–100.
41. Carroll, J.B., Lerch, J.P., Franciosi, S., Spreeuw, A., Bissada, N., Henkelman, R.M. and Hayden, M.R. (2011) Natural history of disease in the YAC128 mouse reveals a discrete signature of pathology in Huntington disease. *Neurobiol. Dis.*, **43**, 257–265.
42. Vonsattel, J.J.P., Myers, R.R.H., Stevens, T.T.J., Ferrante, R.R.J., Bird, E.E.D. and Richardson, E.E.P. (1985) Neuropathological classification of Huntington's disease. *J. Neuropathol. Exp. Neurol.*, **44**, 559–577.
43. Vonsattel, J.P. and DiFiglia, M. (1998) Huntington Disease. *J Neuropathol. Exp. Neurol.*, **57**, 369–384.
44. Bibb, J.A., Yan, Z., Svenningsson, P., Snyder, G.L., Pieribone, V.A., Horiuchi, A., Nairn, A.C., Messer, A. and Greengard, P. (2000) Severe deficiencies in dopamine signaling in presymptomatic Huntington's disease mice. *Proc. Natl. Acad. Sci. U. S. A.*, **97**, 6809–6814.
45. Van Raamsdonk, J.M., Pearson, J., Rogers, D.A., Bissada, N., Vogl, A.W., Hayden, M.R. and Leavitt, B.R. (2005) Loss of wild-type huntingtin influences motor dysfunction and survival in the YAC128 mouse model of Huntington disease. *Hum. Mol. Genet.*, **14**, 1379–1392.
46. Gutekunst, C.A., Li, S.H., Yi, H., Mulroy, J.S., Kuemmerle, S., Jones, R., Rye, D., Ferrante, R.J., Hersch, S.M. and Li, X.J. (1999) Nuclear and neuropil aggregates in Huntington's disease: relationship to neuropathology. *J. Neurosci.*, **19**, 2522–2534.
47. Slow, E.J., Graham, R.K., Osmand, A.P., Devon, R.S., Lu, G., Deng, Y., Pearson, J., Vaid, K., Bissada, N., Wetzel, R. *et al.* (2005) Absence of behavioral abnormalities and neurodegeneration in vivo despite widespread neuronal huntingtin inclusions. *Proc. Natl Acad. Sci. U. S. A.*, **102**, 11402–11407.
48. Kuhn, A., Thu, D., Waldvogel, H.J., Faull, R.L.M. and Luthi-Carter, R. (2011) Population-specific expression analysis (PSEA) reveals molecular changes in diseased brain. *Nat. Methods*, **8**, 945–947.
49. Hodges, A., Strand, A.D., Aragaki, A.K., Kuhn, A., Sengstag, T., Hughes, G., Elliston, L.A., Hartog, C., Goldstein, D.R., Thu, D. *et al.* (2006) Regional and cellular gene expression changes in human Huntington's disease brain. *Hum. Mol. Genet.*, **15**, 965–977.
50. Thomas, E.A. (2006) Striatal specificity of gene expression dysregulation in Huntington's disease. *J. Neurosci. Res.*, **84**, 1151–1164.
51. Runne, H., Regulier, E., Kuhn, A., Zala, D., Gokce, O., Perrin, V., Sick, B., Aebischer, P., Deglon, N. and Luthi-Carter, R. (2008) Dysregulation of gene expression in primary neuron models of Huntington's disease shows that polyglutamine-related effects on the striatal transcriptome may not be dependent on brain circuitry. *J. Neurosci.*, **28**, 9723–9731.
52. Becanovic, K., Pouladi, M.A., Lim, R.S., Kuhn, A., Pavlidis, P., Luthi-Carter, R., Hayden, M.R. and Leavitt, B.R. (2010) Transcriptional changes in Huntington disease identified using genome-wide expression profiling and cross-platform analysis. *Hum. Mol. Genet.*, **19**, 1438–1452.
53. Kuhn, A., Goldstein, D.R., Hodges, A., Strand, A.D., Sengstag, T., Kooperberg, C., Becanovic, K., Pouladi, M.A., Sathasivam, K., Cha, J.H.J. *et al.* (2007) Mutant huntingtin's effects on striatal gene expression in mice recapitulate changes observed in human Huntington's disease brain and do not differ with mutant huntingtin length or wild-type huntingtin dosage. *Hum. Mol. Genet.*, **16**, 1845–1861.
54. Bayram-Weston, Z., Stone, T.C., Giles, P., Elliston, L., Janghra, N., Higgs, G.V., Holmans, P.A., Dunnett, S.B., Brooks, S.P. and Jones, L. (2015) Similar striatal gene expression profiles in the striatum of the YAC128 and HdhQ150 mouse models of Huntington's disease are not reflected in mutant huntingtin inclusion prevalence. *BMC Genomics*, **16**, 14.
55. Hebb, A.L.O., Robertson, H.A. and Denovan-Wright, E.M. (2004) Striatal phosphodiesterase mRNA and protein levels are reduced in Huntington's disease transgenic mice prior to the onset of motor symptoms. *Neuroscience*, **123**, 967–981.
56. Hu, H., McCaw, E.A., Hebb, A.L.O., Gomez, G.T. and Denovan-Wright, E.M. (2004) Mutant huntingtin affects the rate of transcription of striatum-specific isoforms of phosphodiesterase 10A. *Eur. J. Neurosci.*, **20**, 3351–3363.
57. Cha, J.H.J., Kosinski, C.M., Kerner, J.A., Alsdorf, S.A., Mangiarini, L., Davies, S.W., Penney, J.B., Bates, G.P. and Young, A.B. (1998) Altered brain neurotransmitter receptors in transgenic mice expressing a portion of an abnormal human Huntington disease gene. *Proc. Natl Acad. Sci. U. S. A.*, **95**, 6480–6485.
58. Glass, M., van Dellen, A., Blakemore, C., Hannan, A.J. and Faull, R.L.M. (2004) Delayed onset of Huntington's disease in mice in an enriched environment correlates with delayed loss of cannabinoid CB1 receptors. *Neuroscience*, **123**, 207–212.
59. Huang, K., Kang, M.H., Askew, C., Kang, R., Sanders, S.S., Wan, J., Davis, N.G. and Hayden, M.R. (2010) Palmitoylation and function of glial glutamate transporter-1 is reduced in the YAC128 mouse model of Huntington disease. *Neurobiol. Dis.*, **40**, 207–215.
60. Stanek, L.M., Yang, W., Stuart, A., Sardi, S.P., Hayden, M.R., Hung, G., Bennett, C.F., Cheng, S.H. and Shihabuddin, L.S. (2013) Antisense oligonucleotide-mediated correction of transcriptional dysregulation is correlated with behavioral

benefits in the YAC128 mouse model of Huntington's disease. *J. Huntingtons Dis.*, **2**, 217–228.
61. Kwan, W., Magnusson, A., Chou, A., Adame, A., Carson, M.J., Kohsaka, S., Masliah, E., Moller, T., Ransohoff, R., Tabrizi, S.J. *et al.* (2011) Bone marrow transplantation confers modest benefits in mouse models of Huntington's disease. *J. Neurosci.*, **32**, 133–142.
62. Connolly, C., Magnusson-Lind, A., Lu, G., Wagner, P.K., Southwell, A.L., Hayden, M.R., Bjorkqvist, M. and Leavitt, B.R. (2016) Enhanced immune response to MMP3 stimulation in microglia expressing mutant huntingtin. *Neuroscience*, **325**, 74–88.
63. Østergaard, M.E., Kumar, P., Nichols, J., Watt, A., Sharma, P.K., Nielsen, P. and Seth, P.P. (2015) Allele-selective inhibition of mutant huntingtin with 2-thio- and C5- triazolylphenyl-deoxythymidine-modified antisense oligonucleotides. *Nucleic Acid Ther.*, **25**, 266–274.
64. Nasir, J., Floresco, S.B., O'Kusky, J.R., Diewert, V.M., Richman, J.M., Zeisler, J., Borowski, A., Marth, J.D., Phillips, A.G. and Hayden, M.R. (1995) Targeted disruption of the Huntington's disease gene results in embryonic lethality and behavioral and morphological changes in heterozygotes. *Cell*, **81**, 811–823.
65. Pouladi, M.A., Morton, A.J. and Hayden, M.R. (2013) Choosing an animal model for the study of Huntington's disease. *Nat. Rev. Neurosci.*, **14**, 708–721.
66. Menalled, L.B., Kudwa, A.E., Miller, S., Fitzpatrick, J., Watson-Johnson, J., Keating, N., Ruiz, M., Mushlin, R., Alosio, W., McConnell, K. *et al.* (2012) Comprehensive behavioral and molecular characterization of a new knock-in mouse model of Huntington's disease: zQ175. *PLoS One*, **7**, e49838.
67. Southwell, A.L., Smith-Dijak, A., Kay, C., Sepers, M., Villanueva, E.B., Parsons, M.P., Xie, Y., Anderson, L., Felczak, B., Waltl, S. *et al.* (2016) An enhanced Q175 knock-in mouse model of Huntington disease with higher mutant huntingtin levels and accelerated disease phenotypes. *Hum. Mol. Genet.*, **25**, 3654–3675.